NMDAR-mediated transcriptional control of gene expression in the specification of interneuron subtype identity

Vivek Mahadevan[a], Apratim Mitra[b], Yajun Zhang[c], Areg Peltekian[a], Ramesh Chittajallu[a], Caraoline Esnault[b,1], Dragan Maric[d], Christopher Rhodes[c], Kenneth A. Pelkey[a], Ryan Dale[b], Timothy J. Petros[c], Chris J. McBain[a,*]

[a]*Section on Cellular and Synaptic Physiology, Eunice Kennedy Shriver National Institute of Child Health and Human Development (NICHD), Bethesda, 20892, MD, USA*
[b]*Bioinformatics and Scientific Programming Core, NICHD, Bethesda, 20892, MD, USA*
[c]*Unit on Cellular and Molecular Neurodevelopment, NICHD, Bethesda, 20892, MD, USA*
[d]*Flow and Imaging Cytometry Core Facility, National Institute of Neurological Disorders and Stroke (NINDS), Bethesda, 20852, MD, USA*

Abstract

Medial ganglionic eminence (MGE)-derived parvalbumin (PV)+, somatostatin (SST)+ and Neurogliaform (NGFC)-type cortical and hippocampal interneurons, have distinct molecular, anatomical and physiological properties. However, the molecular mechanisms regulating their diversity remain poorly understood. Here, via single-cell transcriptomics, we show that the obligate NMDA-type glutamate receptor (NMDAR) subunit gene *Grin1* mediates subtype-specific transcriptional regulation of gene expression in MGE-derived interneurons, leading to altered subtype identities. Notably, MGE-specific conditional *Grin1* loss results in a systemic downregulation of diverse transcriptional, synaptogenic and membrane excitability regulatory programs. These widespread gene expression abnormalities mirror aberrations that are typically associated with neurodevelopmental disorders, particularly schizophrenia. Our study hence provides a road map for the systematic examination of NMDAR signaling in interneuron subtypes, revealing potential MGE-specific genetic targets that could instruct future therapies of psychiatric disorders.

Keywords: Interneurons, Medial ganglionic eminence, PV, SST, Neurogliaform, NMDA receptor, Transcriptional regulation, Neurodevelopmental disorders, Schizophrenia, NMDA-hypofunction, Hippocampus, Frontal Cortex, Mouse model, scRNAseq

Email addresses:
vivek.mahadevan@nih.gov (Vivek Mahadevan),
ryan.dale@nih.gov (Ryan Dale),
tim.petros@nih.gov (Timothy J. Petros),
mcbainc@mail.nih.gov (Chris J. McBain) *Corresponding author.

Introduction

Medial ganglionic eminence (MGE)-derived forebrain GABAergic interneurons comprise the parvalbumin-containing (PV) and somatostatin-containing (SST) subpopulations throughout the entire forebrain accounting for approximately 60% of all cortical interneurons [1, 2]. In addition, approximately half of all hippocampal neurogliaform-type cells (NGFCs), the so called Ivy cells, originate from the MGE [3, 4]. Interestingly, though only rarely found in rodent neocortex such MGE-derived NGFCs are significantly more populous in primate neocortex, including humans [5]. While PV neurons exert robust somatic, and proximal dendritic inhibition, the SST and NGFCs mediate domain-specific dendritic inhibition on their downstream pyramidal neuron targets [6]. Collectively these classes of interneurons shape diverse aspects of cortical and hippocampal circuit maturation during development, and critically regulate information processing in mature circuits by maintaining appropriate excitation-inhibition (E-I) balance [7]. Recent evidence indicates a critical role for activity, particularly through ionotropic glutamate receptors (iGluRs), in driving the morpho-physiological maturation of MGE-derived interneurons [8–12]. Unlike mature interneurons where iGluRs differentially contribute towards synaptic transmission, immature and migrating interneurons express different glutamate receptor subunits including the NMDA-type iGluR (NMDAR) and AMPA/Kainate-type iGluR (AMPAR/KAR) [13–15] prior to the expression of any functional synapses. This becomes particularly important as the developing brain contains higher ambient glutamate levels than the adult brain [16]. Collectively, higher ambient glutamate, developmental expression of iGluRs and recruitment of glutamatergic signaling is considered to be trophic [8, 17, 18] and thought to engage mechanisms to regulate various aspects of interneuron development including morphological and electrical maturation to promote appropriate circuit integration [9, 11, 14, 16, 19–22].

Interneuron-specific impairments are increasingly considered central to the etiology of multiple neurodevelopmental and circuit disorders [23]. The importance of interneuron-expressed iGluRs is most notable in psychiatric disorders exhibiting impaired NMDAR-associated systems [24, 25]. In the adult brain, acute pharmacological NMDAR blockade results in circuit disinhibition and psychotic symptoms [26], mediated in-part, by the enhanced sensitivity of interneuronal NMDARs to their antagonists [27]. Indeed, direct blockade of interneuron activity also precipitates distinct behavioral deficits relevant to schizophrenia [28]. In particular, ablation of the obligate NMDAR subunit gene *Grin1* in interneuron-specific early postnatal mouse [29], but not PV-specific [30], or glutamatergic neuron-specific *Grin1* ablation [31], resembles global *Grin1*-mutants [32] in their constellation of schizophrenia-like behavioral aberrations. This indicates that *Grin1* dysfunction across multiple interneuron-subtypes precipitates schizophrenia-like abnormalities [33]. In addition, this interneuron-specific NMDAR-hypofunction model is sensitive to developmental age, since adult-onset *Grin1* loss does not result in the same phenotypes [29]. Despite the importance of developmental NMDAR function in interneurons, and its relevance to human neurodevelopmental disorders, a comprehensive interrogation of the impact of developmental NMDAR ablation in interneurons, particularly across MGE-derived interneurons, is lacking.

It is clear that during the developmental window between embryonic day (ED) 13.5 and

postnatal day (PD) ~10 [34], a combination of innate genetic programs, external environment, and neuronal activity shapes interneuron subtype specification leading to remarkable diversity [2, 21, 35, 36] The NMDAR signaling complex comprises an essential node for regulating gene expression via excitation-transcription (E-T) coupling in mature circuits [37–39]. Moreover, different NMDAR subunits are widely expressed in the developing brain [40] where they provide a critical source of Ca^{2+}-entry via trophic glutamate signaling prior to synaptogenesis [15, 19, 41]. However, it is not clear whether the NMDAR-mediated Ca^{2+} cascades in nascent and developing MGE-derived interneurons engage transcriptional programs necessary for MGE-derived interneuron diversity. To investigate this, we conditionally deleted *Grin1* in MGE progenitors that give rise to cortical and hippocampal PV, SST, and NGFC subsets, using the *Nkx2-1*-Cre mouse line [3, 4, 42]. In this model, *Nkx2-1*-driven Cre expression is reported in cycling/proliferating MGE cells, well before the cells become postmitotic, allowing for assessment of the developmental impact of embryonic loss of *Grin1* activity across all subsets of MGE-derived interneurons. Applying high-throughput single-cell RNA sequencing (scRNAseq), we establish that NMDAR-mediated transcriptional cascades promote MGE subtype identity, by regulating the expression of diverse transcriptional, synaptogenic and membrane excitability genetic programs. Notably, we identify numerous disease-relevant genes that are misexpressed in MGE-derived interneurons upon *Grin1*-ablation, providing a broad road map for examination of MGE-subtype specific regulation via NMDAR signaling.

Results

scRNAseq recapitulates cardinal MGE subtypes and a continuum of molecular profiles

To examine the molecular heterogeneity of MGE-derived GABAergic interneurons by scRNAseq, we microdissected frontal cortex (CX) and hippocampus (HPC) from fresh brain slices obtained from PD18-20 *Nkx2.1*-Cre:Ai14 mouse **(Figure1A, Figure1-Supplement1A)**. Ai14-TdTomato (TdT^+) single-cell suspensions were harvested by fluorescence-activated cell sorting (FACS) using stringent gating constraints including viability and doublet discrimination **(Figure1-Supplement1B)** as previously described [43–45], and subsequently processed through the 10X Genomics Chromium controller. 9064 and 9964 TdT^+cells were recovered from cortex and hippocampus respectively across 3 biological replicates. To minimize the effect of excitotoxicity and stress-related transcriptional noise, the tissue processing, FACS, and sample collection steps were performed in buffers supplemented with Tetrodotoxin (TTX), DL -2-Amino-5-phosphonopentanoic acid (APV) and Actinomycin-D (Act-D) [46]. Because we observed concordant cell clustering across the replicates during preliminary analysis by Seurat v3 [47, 48] **(Figure1-Supplement2A)**, the replicates were pooled for in-depth analysis. Subsequent clustering and marker gene analyses revealed that ~ 62% and 33% of the TdT^+ MGE-sorts from cortex and hippocampus respectively, express classical GABA markers including *Gad1 / Gad2*, *Lhx6*; and the MGE-subclass markers *Pvalb*, *Sst*, and *Lamp5*, marking PV and SST, NGFC subsets respectively **(Figure1B, Figure1-Supplement3A)**. While we did not recover cells expressing

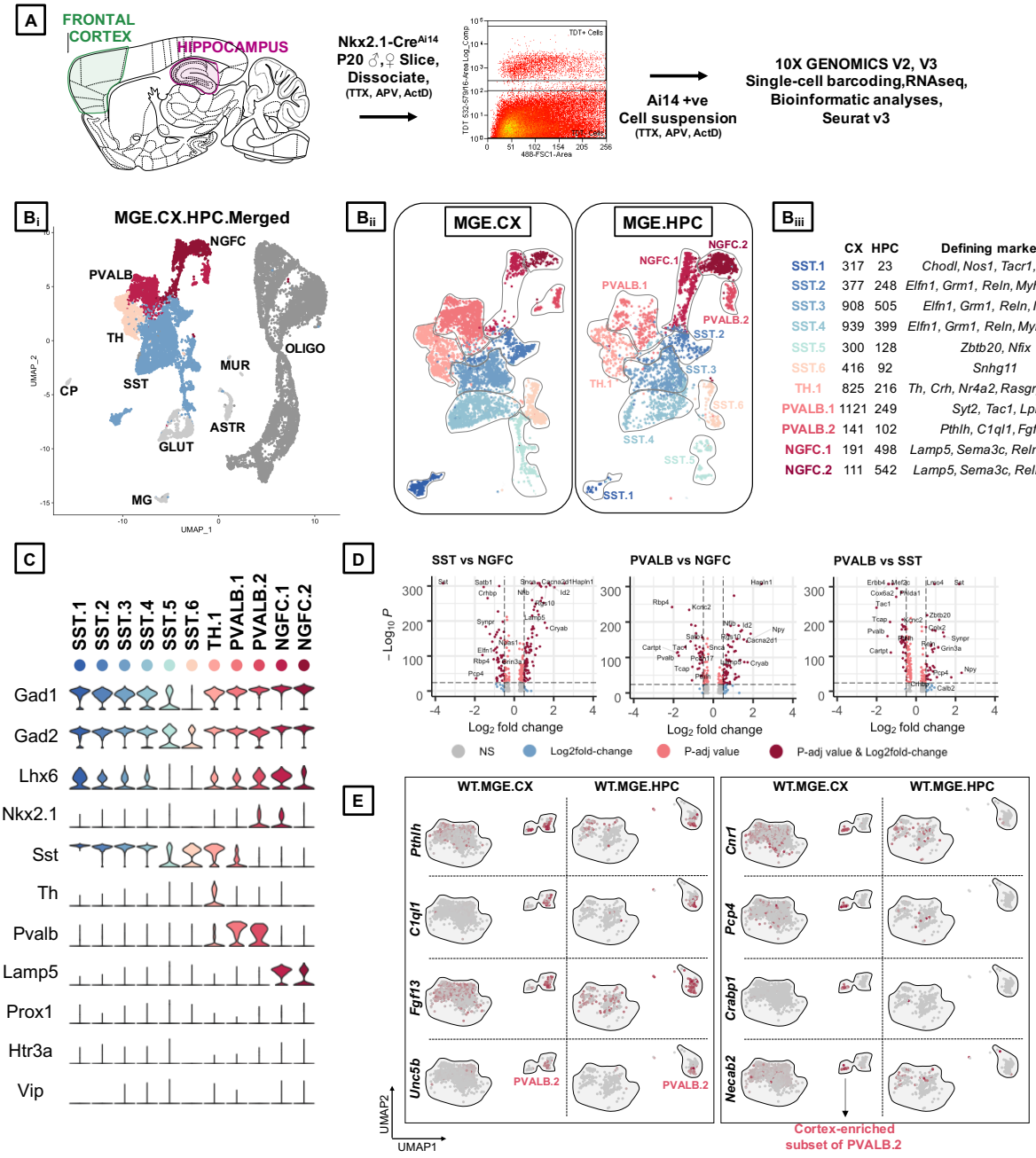

Figure 1: **Identification of MGE-derived interneuron subtypes in the cortex and hippocampus. A,** Overview of the experimental workflow. $\mathbf{B}_i$**,** Uniform Manifold Approximation and Projection (UMAP) dimensional reduction of 19,028 single-cell transcriptomes (9,064 from frontal cortex and 9,964 from hippocampus of 6 mouse brains), showing the cardinal MGE populations. Cell clusters were color coded and annotated *post hoc* based on their transcriptional profile identities (Cell type abbreviations: PVALB, Parvalbumin; NGFC, Neurogliaform; TH, Tyrosine Hydroxylase; SST, Somatostatin; GLUT, Glutamatergic; CP, Choroid Plexus; MG, Microglia; ASTR, Astrocyte; MUR, Mural; OLIGO, Oligodendrocyte). $\mathbf{B}_{ii}$**,** UMAP visualization of 11 MGE-derived interneuron subtypes from cortex (MGE.CX) and hippocampus (MGE.HPC), and the recovery of cell numbers from the subtypes. $\mathbf{B}_{iii}$**,** Table indicating the number of *Gad1/Gad2*$^+$cells recovered in each MGE subtype from the cortex and hippocampus, and the defining genes enriched in each subtype. **C,** Violin plot showing the distribution of expression levels of well-known representative cell-type-enriched marker genes across the11 MGE subtypes. **D,** −log10 False Discovery Rate (FDR) versus log2 fold change (FC) between each of the MGE cardinal class, representing the top enriched markers at a fold change $\geq$0.5 and FDR $<$10e-25. **E,** UMAP representation of PVALB clusters highlighting the cortex-specific enrichment of *Pthlh*-expressing PVALB.2 subtype that is not observed in the hippocampus.

the CGE-markers *Prox1*, *Htr3a* or *Vip*, we recovered a minor fraction of cells corresponding to glutamatergic neurons, astrocytes and microglia. In addition, ~25% and 71% TdT^+ MGE-sorts from cortex and hippocampus respectively were enriched in oligodendrocytes marked by *Olig1* expression across all replicates **(Figure1-Supplement 2B,2C)**. However, we focused our subsequent analyses on the 5656 and 3002 *Gad1 / Gad2* positive cortical and hippocampal MGE-derived interneurons.

Unbiased cell clustering by Seurat v3 identified six subtypes of SST, two subtypes of PV, two subtypes of NGFCs, and one subtype of Tyrosine hydroxylse (TH) expressing interneurons, expressing the markers *Sst*, *Pvalb*, *Lamp5* and *Th* respectively, across the two brain regions examined **(Figure1C)**. Notably, all but two subtypes (SST.5 and SST.6) expressed high levels of *Lhx6*, and 2 clusters corresponding to PV.2 and NGFC.1 expressed *Nkx2.1* at this developmental time. While the PV- SST- and NGFC- clusters clearly exhibited robust gene expression differences among each other **(Figure1D)**, the TH cluster appeared to express genes that correspond to both PV: SST clusters, including *Sst* and *Pvalb* expressions **(Figure1C, Figure1-Supplement3B)**. Particularly, at this developmental window we could not observe robustly different gene expression variances between the cortical and hippocampal counterparts, barring a few marginal, but significant differences **(Figure1-Supplement4B) .** This gave us sufficient rationale to perform subsequent analyses using the MGE-derived interneurons pooled from cortex and hippocampus.

Among the **SST sub clusters**, SST.1-5 uniquely expresses *Chodl*, *Igf2bp3*, *Cdh7*, *Pld5* and *Nfix* respectively, while SST.6 expresses only markers that are common with other SST clusters **(Figure1-Supplement3B)**. With the exception of SST.6 the remaining SST-expressing subclusters are described in previous scRNAseq assays **(Figure1-Supplement5A)**. For example, the *Chodl*-expressing SST.1 cluster co-express high *Nos1, Tacr1, Penk,* and *Npy*, and it has been previously described as putative GABAergic long-range projections neurons [49, 50]. Clusters SST.2/3/4 express *Elfn1*, *Reln* and *Grm1* characteristic of putative cortical martinotti and their hippocampal counterpart, oriens-lacunosum/moleculare (O-LM) [43, 51, 52]**(Figure1-Supplement5B)**. Lastly, *Zbtb20*-expressing SST.5 is predicted to be septal-projecting interneurons [43]. Among the **PV sub clusters**, while both PVALB.1&2 coexpresses several common markers including *Pvalb*, *Kcnip2*, *Tcap* and *Kcnc1* there are several notable differences between the two clusters. PVALB.1 appears to contain continuous, but non-overlapping populations expressing *Syt2* representing putative fast-spiking basket cells or *Rbp4/Sst* containing putative bistratified cells [1, 43, 53]**(Figure1-Supplement5D)** . PVALB.2 contains cells that uniquely expresses *Pthlh*, *C1ql1, Fgf13* and *Unc5b* representing putative axo-axonic chandelier cells [43, 49, 54]. We also observed a TH cluster, which, in addition to expressing several genes common to the SST: PV clusters, expresses several unique genes including *Rasgrp1*, *Bcl6*, *Myo1b* that segregated into mutually exclusive cluster space expressing *Crh* or *Nr4a2* **(Figure1-Supplement3B, Figure1-Supplement5B)** . This cluster is also described previously as putative bistratified-like cells [43, 53] . Among the **NGFC sub clusters**, while both NGFC.1&2 coexpress several common markers including *Lamp5, Hapln1, Cacna2d1, Sema3c* and *Id2*, the NGFC.1 cluster uniquely expresses several genes like *Reln, Ngf, Egfr, Gabra5* that are not expressed by NGFC.2. **(Figure1-Supplement3B)**. While the *Reln*+

represents MGE-derived neurogliaforms, the *Reln*-population may represent putative ivy cells [43] **(Figure1-Supplement5C)**.

While the majority of the UMAP space aligns well between the cortical and hippocampal MGE-derived interneurons, we observed some regional differences as well. **(Figure1-Supplement3A$_i$A$_{iii}$)**. (i) First, we observed an increase in the HPC-expressed NGFC.1&2 in comparison to their cortical counterparts, consistent with preferential localization of MGE-derived NGFCs to HPC over CX in rodents [1, 3, 4]. (ii) Next, the *Pthlh*-expressing PVALB.2 subcluster splits into two islands, only in the cortex and distinctly lacking from the hippocampus. Only one of the PVALB.2 islands expresses *C1ql1*, while the other cortex-enriched island expresses unique markers *Etv1*, *Cnr1*, *Pcp4*, *Crabp1*, *Necab2, Epha4, Crabp1* and *Hapln1* **(Figure1E, Figure1-Supplement5D)** . Whether this represents a novel subclass of chandelier cells remains to be determined. (iii) Lasty, we also observed a distinction in the hippocampal SST.3 corresponding to a subset of O-LM interneurons **(Figure1-Supplement3A$_{ii}$)**. The overall MGE cell numbers indicate that the SST cells account for the majority of MGE cell population recovered in the scRNAseq assay from both brain regions **(Figure1-Supplement3A$_{ii,}$ A$_{iii}$)**. The PV and TH clusters accounted for a greater share of MGE-derived interneurons in the CX than in the HPC. While it is plausible these relative cell proportions may be skewed by differential survivability of these subtypes during tissue dissociation, sorting and single-cell barcoding, these relative percentages were similar across biological replicates.

NMDAR signaling maintains MGE identities and subtype diversity

Because neuronal activity and glutamatergic signaling are known to regulate multiple facets of interneuronal development [2, 21] [11, 36, 55] , we hypothesized that the key obligate subunit *Grin1* and the NMDAR signaling complex may play an instructive role in determining MGE subtype identities. To test whether NMDAR signaling impact the development and function of MGE-derived interneurons, we ablated them in MGE progenitors by crossing floxed-*Grin1* mice with the *Nkx2.1*-Cre mouse line [42]. The Earliest expressions of *Nkx2.1* and *Grin1* in the developing rodent brains occur around ~embryonic day (ED) 10.5 and ~ED14 respectively [56–58]. Moreover, NMDAR-mediated Ca^{2+} signaling in migrating interneurons are reported by ~ED16 [15]. Because the expression and activity of *Nkx2.1* precedes *Grin1* expression, we rationalized that utilizing *Nkx2.1*-Cre mouse will ablate *Grin1* and NMDAR signaling in MGE progenitors from the earliest developmental point. We sorted TdT^+cells from the cortex and hippocampus of *Nkx2.1*-Cre:*Grin1*$^{fl/fl}$:Ai14 mice and performed scRNAseq using the 10X platform. The scRNAseq experiments were performed using juvenile mice (PD18-20) of both sexes and from the same litters as the wildtypes (WT) to enable subsequent direct comparison. Similar to the WT-datasets, the MGE-*Grin1*$^{fl/fl}$ mutants also revealed an enrichment of TdT^+ oligodendrocytes **(Figure2-Supplement3B)**, however, we again focused our attention on the *Gad1/2* positive interneurons.

We next performed integrated analyses of the MGE-*Grin1*^{wt}and MGE-*Grin1*$^{fl/fl}$cortical and hippocampal scRNAseq datasets. Applying similar unbiased clustering parameters used for the MGE-*Grin1*^{wt}analyses, we observed a total of twelve *Gad1/2* positive clusters in the integrated dataset **(Figure2A, B).** As a robust control, *Grin1* appeared to be absent or vastly reduced in all MGE subsets in both brain regions from MGE-*Grin1*$^{fl/fl}$ **(Figure2C),**

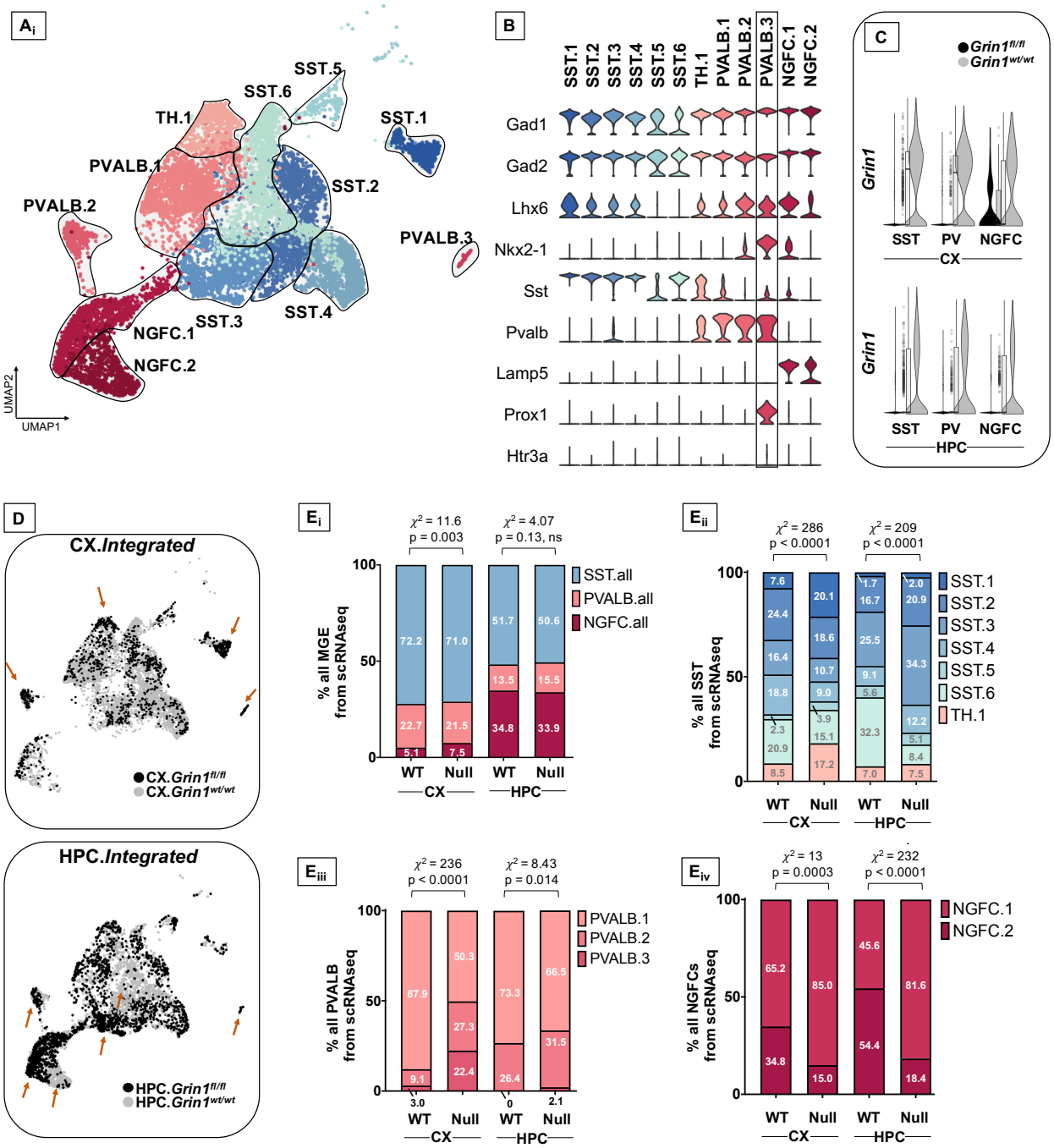

Figure 2: **Altered interneuron subtype proportions upon *Grin1*-ablation**
A, Integrated UMAP visualization of 12 subtypes of MGE-derived interneurons obtained from cortex (CX) and hippocampus (HPC) of $Grin1^{wt/wt}$ and $Grin1^{fl/fl}$mice **B,** Violin plot showing the distribution of expression levels of well-known representative cell-type-enriched marker genes across the 12 interneuron subtypes. **C,** Violin plot from both genotypes indicating the expression of *Grin1* in the cardinal of MGE-derived interneuron subtypes. **D,** UMAP representation colored by brain-region, highlighting the differential enrichments of cells (brown arrows) within interneuron subsets in *Grin1*-WT and *Grin1*-null from CX and HPC. **E,** Stacked-barplots representing the proportions of recovered cell numbers within $\mathbf{E}_i$, pooled cardinal MGE subtypes, $\mathbf{E}_{ii}$, SST subtypes; $\mathbf{E}_{iii}$, PVALB subtypes and $\mathbf{E}_{iv}$, NGFC subtypes in *Grin1*-WT and *Grin1*-null from cortex or hippocampus. χ^2, Chi-square test of proportions; ns, not significant.

but not in the *Slc17a7* expressing glutamatergic neurons **(Figure2-Supplement3A)**. Overlaying the WT and NULL datasets from the brain regions revealed differential enrichments among the recovered cells between the genotypes **(Figure2D)**. Intriguingly, *Grin1*-ablation did not seem to alter the SST or PV recovery percentages, with the exception of a modest increase in the cortical NGFCs (χ^2 = 11.6, p = 0.003), but not hippocampal NGFCs (χ^2 = 4.07, p = 0.13) **(Figure2E$_i$, Figure2-Supplement2A$_i$,B).** However, we observed a marked change in the recovery percentages of the subsets of SST, PV and NGFCs from both cortex and hippocampus **(Figure2E$_{ii-iv}$, Supplement2A$_{ii}$,C)**. Particularly, we observed a robust increase in the *Chodl*-expressing cortical SST.1 population, and a decrease in hippocampal SST.6 population in MGE-*Grin1*$^{fl/fl}$(CX, HPC: χ^2 = 286, 209; p-value = 2.2e-16 for both regions). In addition, we found a reduction in the cortical PVALB.1 population, and a compensatory increase in PVALB.2/3 populations in MGE-*Grin1*$^{fl/fl}$(CX, HPC: χ^2 = 236, 8.4; p-value = 2.2e-16, 0.14). Finally, we observed an increase in the NGFC.1 along with a compensatory decrease in NGFC.2 in both cortex and hippocampus (CX, HPC: χ^2 = 13, 232; p-value = 0.0003, 0.14).

To independently examine whether *Grin1* ablation promotes changes in interneuron abundances, we conducted immunostaining experiments to probe total TdT$^+$ MGE-derived interneurons and the PV / SST subtypes. First, we observed no significant change in total TdT$^+$ hippocampal MGE-derived interneuron density between postnatal day (PD) 30-210 **(Figure2-Supplement1A$_i$)** similar to what was indicated in the scRNAseq cell recoveries **(Figure2E$_i$)**. Next, we observed a modest decrease in cortical TdT$^+$ numbers at PD30, which became progressively greater by PD210 **(Figure2-Supplement1B$_i$)**, indicating different effects of *Grin1*-ablation on total MGE cell numbers in cortex and hippocampus. We observed no change in hippocampal expressed total PV/SST cell type counts at PD30 **(Figure2-Supplement1A$_{ii}$)**, but we noted a modest reduction in cortical PV cell type counts along with an increase in cortical SST cell type counts at the same age **Figure2-Supplement1Bi$_i$)**.

Among the differentially enriched subclusters, *Pthlh*-expressing PVALB.3 is quite notable **(Figure2B, Figure2-Supplement3A,B)**. This cortex-enriched cluster lacking in the hippocampus was identified within the PVALB.2 putative-chandelier cells in the MGE-*Grin1*$^{wt/wt}$ **(Figure1E, Figure1-Supplement5D)**, However, subsequent to integration of the MGE-*Grin1*$^{fl/fl}$ scRNAseq dataset, it segregated as a unique cluster, far from other PVALB clusters in the UMAP space. We observed *Prox1* expression in PVALB.3, which is uncharacteristic of MGE-derived interneurons, additional to robust expressions of genes associated with NGFCs such as *Hapln1* and *Reln* **(Figure2-Supplement3A,B)**. Moreover, we observed an increase in recovery of the cortical PVALB.3 cell numbers, including the emergence of these cells in the hippocampus subsequent to *Grin1*-ablation **(Figure2-Supplement2A,B).** It is unclear whether the changes in marker expression reflect a true change in cell identity or whether this is reflective of alterations in relative interneuron subtype proportions. Nevertheless, these data demonstrate clear changes in MGE-derived interneuron subtype diversity following loss early embryonic loss of *Grin1* function.

NMDAR signaling shapes the transcriptional landscape in MGE-derived interneurons

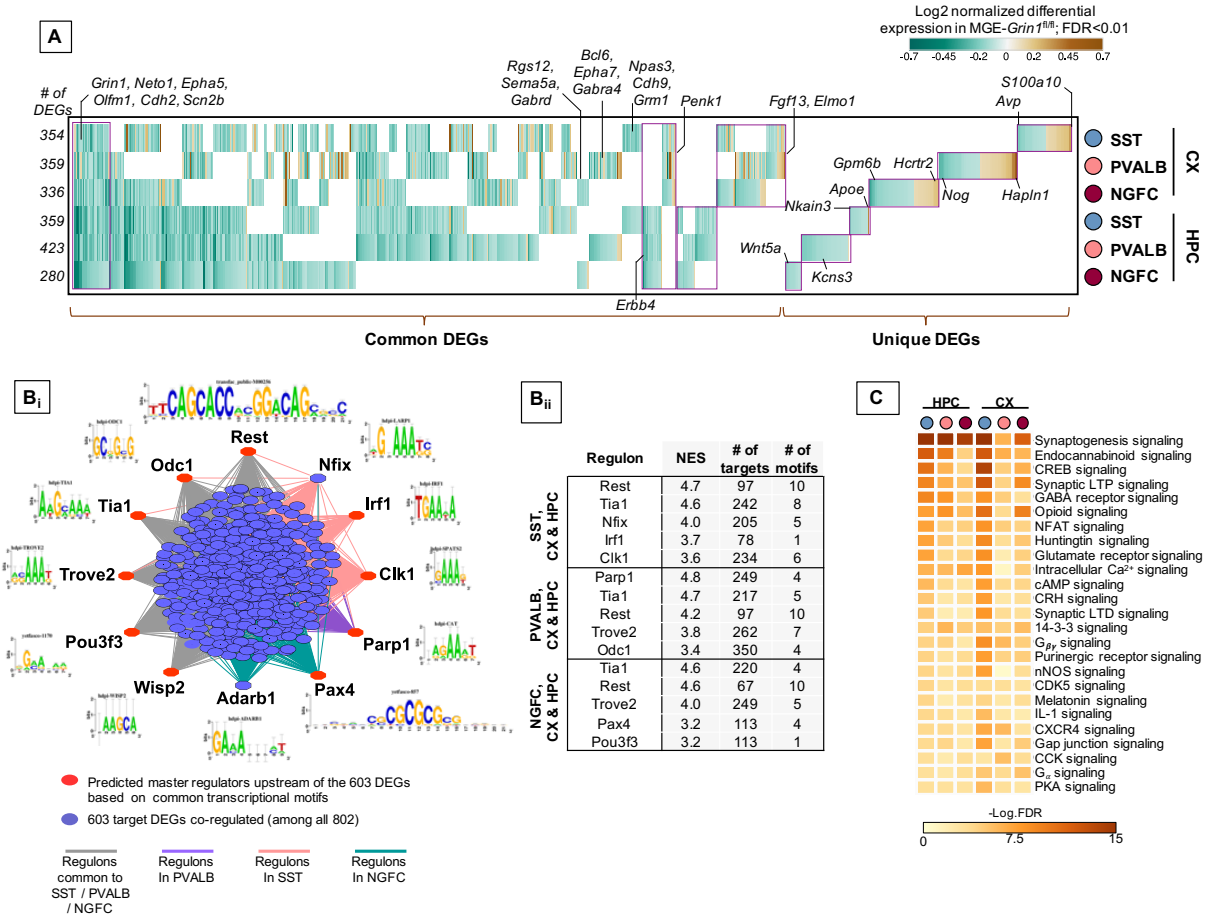

	Regulon	NES	# of targets	# of motifs
SST, CX & HPC	Rest	4.7	97	10
	Tia1	4.6	242	8
	Nfix	4.0	205	5
	Irf1	3.7	78	1
	Clk1	3.6	234	6
PVALB, CX & HPC	Parp1	4.8	249	4
	Tia1	4.7	217	5
	Rest	4.2	97	10
	Trove2	3.8	262	7
	Odc1	3.4	350	4
NGFC, CX & HPC	Tia1	4.6	220	4
	Rest	4.6	67	10
	Trove2	4.0	249	5
	Pax4	3.2	113	4
	Pou3f3	3.2	113	1

Figure 3: **Cell-autonomous transcriptional changes subsequent to MGE-specific developmental *Grin1*-ablation** **A,** Combined heatmap representing the 802 differentially expressed (DEGs) in the cortical and hippocampal MGE-derived interneurons upon *Grin1*-ablation, at a FDR<0.01 and FC>10%, as determined by MAST analysis (see details in Methods). $\mathbf{B}_i$**,** iRegulon *in silico* analysis identifying high-confidence master upstream transcriptional regulators(indicated in red) of the DEGs (indicated in lavender). Representative DNA-binding motifs are indicated next to the transcriptional regulators. $\mathbf{B}_{ii}$**,** Top five transcriptional regulators predicted by iRegulon, associated normalized enrichment score (NES) and number of predicted targets and motifs associated with each transcription factor cluster, indicated for the three interneuron subtypes (CX and HPC pooled). **C,** Ingenuity Pathway Analysis of significantly overrepresented molecular pathways in each MGE-subtype.

It is now well-established that transcriptional signatures defines the subtype identities of GABAergic interneurons [59]. To examine the full range of transcriptional impairments triggered by *Grin1* ablation in MGE-derived interneurons, we next performed differential gene expression testing by pooling the SST / PVALB / NGFC subtypes into their cardinal MGE classes to identify the genes that are differentially expressed between the genotypes. For instance SST1-7 and TH.1 are pooled together as SST; PVALB1-3 are pooled together as PVALB, and NGFC1-2 are pooled together as NGFC cardinal classes for this assay . At a stringent false-discovery rate (FDR) <0.01, 802 genes passed the 10%-foldchange (FC)

threshold across the MGE subtypes from both brain regions **(Figure3A, Supplemental Table1)**. Several interesting features were observed in the differentially expressed gene (DEG) pattern upon MGE-specific *Grin1*-ablation. (i) Among all DEGs only ~10% and 1% are upregulated in the cortex and hippocampus respectively, while the remaining genes were all downregulated **(Figure3-Supplement1A$_{ii}$,B,C)**. (ii) While *Grin1* ablation resulted in several unique DEGs between the MGE classes, ~10 and 27% of the DEGs are common within cortex and hippocampus respectively **(Figure3A, Figure3-Supplement2)**. For instance, while *S100a10, Hapln1, Hcrt2* are uniquely upregulated in cortical SST, PV and NGFC respectively **(Figure3A)**, *Apoe, Kcns3, Wnt5a* were uniquely altered in hippocampal SST, PV and NGFC respectively. In contrast, *Grin1* ablation induced common changes in *Penk1* and *Erbb4* expression patterns across all MGE-derived interneuron classes in the cortex and hippocampus respectively. (iii) ~27-43% of all DEGs were shared by MGE classes across brain regions **(Figure3-Supplement2A$_{ii}$)**. For example, *Npas3, Cdh9, Grm1* are commonly downregulated in all SST subclasses; *Bcl6, Epha7, Gabra4* common to PV class; and *Rgs12, Gabrad, Sema5a* common to NGFCs from both brain regions. (iv) Lastly, 28 genes are commonly differentially expressed across both brain regions, across all MGE subtypes. For example, *Grin1, Neto1, Cdh2, Scn2b* are commonly downregulated across the board, while *Epha5, Olfm1* are commonly downregulated across all, but cortical PV cells **(Figure3A)**.

Gene expression co-regulation is intrinsic to cellular diversity [60, 61]. Since the majority of DEGs are downregulated across the MGE subtypes, we examined whether they correspond to clusters of coordinated co-regulation. We applied the iRegulon *in silico* framework [62], which identifies transcription factor binding motifs that are enriched in genomic regions of the DEGs upon *Grin1*-ablation, and predicts the transcription factors that bind to the motifs. This *in silico* analysis predicted 51 significantly enriched motifs (normalized enrichment score > 3) that clustered into 10 groups by similarity, 33 of which were associated with transcription factors **(Figure3B**, **Supplemental Table2)**. Put together, 10 transcription factors were predicted to bind with the motifs with high confidence, strongly supporting targeted co-regulation of 617 among the 802 DEG genes upon *Grin1*-ablation. Notably, the RE1-silencing transcription factor (*Rest*) is a master transcriptional repressor that mediates the transcriptional accessibility for several synaptic genes [63], including NMDAR subunits themselves [64]. It is intriguing to observe that the downregulation of the DEGs upon MGE-specific *Grin1*-ablation are, in part, predicted to occur via *Rest*-mediated transcriptional repression.

To examine the broad biological impact of the DEGs, we performed Gene Ontology (GO) analyses. Broad GO analyses on all DEGs indicates that these genes serve to regulate multiple molecular functions in interneurons, including regulation of GABAergic and glutamatergic synapses, additional to biological pathways related to addiction and circadian entrainment **(Figure3-Supplement2B).** Further classification of DEGs based on their cellular functions within the MGE subtypes revealed genes critical for regulation of membrane excitability, gene expression, synaptic partnering and assembly, as well as major intracellular Ca^{2+} signaling cascades and second messengers **(Figure3C, Figure3-Supplement2C, Supplemental Table3) .**

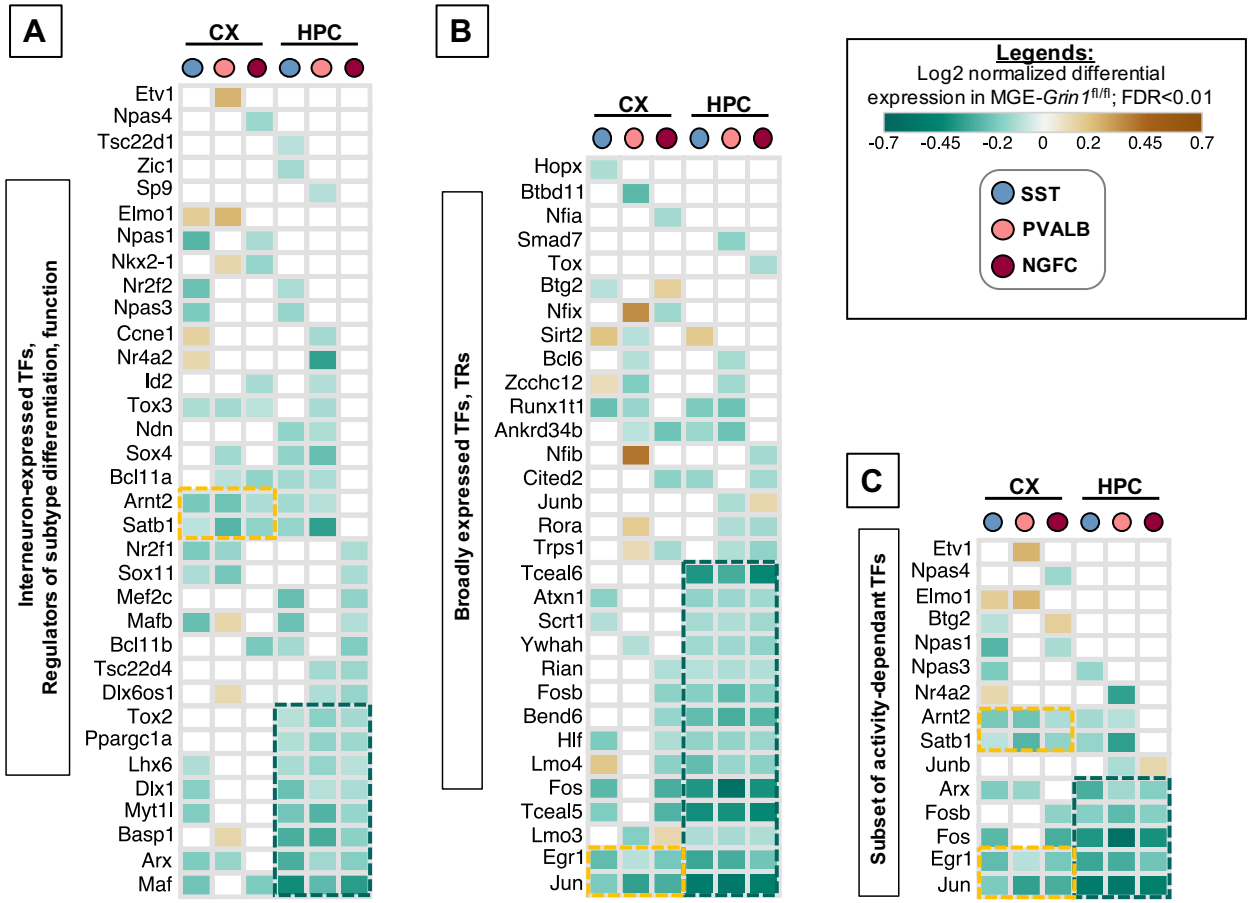

Figure 4: ***Grin1*-signaling in MGE-derived interneurons are highly dedicated to the transcriptional control of interneuron identity** Heatmap of log2 FC of significant DEGs in cortical and hippocampal MGE cardinal subtypes, showing a subset of $\mathbf{A}_i$, Transcription factors (TFs) that are previously established to regulate MGE subtype identity and function; $\mathbf{B}_i$, broadly expressed TFs and transcriptional regulators (TRs) that are not currently known to regulate MGE function; $\mathbf{C}_i$, neuronal activity-regulated TFs. Clusters of commonly differentially expressed genes in cortex and hippocampus are indicated in yellow or green boxes.

Transcription factor expression is a key component of NMDAR-mediated MGE regulation

Because transcriptional regulation underlies numerous fundamental processes including the expression of other classes of genes, we next examined the DE-transcriptional regulators in detail. We first examined the 67 genes that are differentially expressed upon *Grin1*-ablation and are known to mediate transcriptional regulation of gene expression. Of these, 35 genes are previously established to be expressed in different GABAergic interneuron classes including some notable MGE-expressed transcription factors **(Figure4A$_i$)**. The remaining 32 are broadly expressed TFs **(Figure4B$_i$)**, that include a small subset of 15 genes that are regulated by neuronal activity **(Figure4C$_i$)**. Barring a few genes, we observed the majority of TFs to be down regulated in both brain regions. Intracellular Ca^{2+} sig-

naling cascades and second messenger systems are key mediators of NMDAR signaling to the nucleus for transcriptional regulation. Theoretically, an early first wave impairment of Ca^{2+} signaling in *Grin1*-lacking MGE progenitors could result in transcriptional silencing of the mediators of Ca^{2+} signaling cascades and second messenger systems, which would sustain the transcriptional impairments. Indeed, we also observed a downregulation of various Ca^{2+} homeostasis-regulators, kinases / phosphatases and second messengers that are activated downstream of *Grin1* **(Figure4-Supplement1A,B,C)**. Furthermore, we noted that hippocampal MGE neurons had a greater proportion of DE-TFs and kinase signaling cascade effectors that were downregulated across all 3 subtypes compared to their cortical counterparts. Together, this suggests that hippocampal MGE-derived interneurons may be more vulnerable than cortical MGE-derived interneurons towards *Grin1*-mediated Ca^{2+} transcriptional silencing at this age.

Interestingly, among the early TF cascades in the progenitors that sequentially determine and maintain MGE fate, several members appear to be expressed at ~P20, and starkly downregulated upon *Grin1*-ablation. For instance, *Lhx6, Maf, Arx, Myt1l, Dlx1* are among the genes broadly downregulated across all hippocampal MGE subtypes and within specific class(es) in their cortical parallels **(Figure4A$_{ii}$)**. Other MGE fate-determining TFs, *Nkx2-1, Mafb, Satb1, Nr2f1* (CoupTf1), *Sp9*, also appear to be downregulated in discrete populations. This also includes a downregulation of *Bcl11b* (Ctip2) in both hippocampal and cortical NGFCs, a gene recently linked to regulation of NGFC morphology and function [65]. Among the few transcriptional regulators upregulated are *Sirt2, Elmo1, Zcchc12,* none of which have been characterized in the context of MGE function **(Figure4B$_{ii}$)**. *Sirt2* is an established transcriptional repressor [66, 67] that may regulate the repression of several target genes in an MGE-specific manner, and *Elmo1* has been previously characterized during the activity-dependent migration of CGE subtypes [21]. Finally, a recent study has predicted that the expression of *Zcchc12* correlates with slower intrinsic firing among hippocampal CA1 interneurons [43]. This suggests that increased *Zcchc12* expression might regulate the expression of synaptic genes enabling reduced intrinsic excitability in the MGE subsets. Related to such putative decreased excitability in the MGE-derived interneurons, among the activity-regulated TFs, we observe broad downregulation of *Jun, Egr1, Fos, Fosb, Arc, Satb1, Arnt2* across all classes of MGE in both brain regions **(Figure4C$_{ii}$)**. While most of these are well-established activity-regulated TFs, *Arnt2* has been recently described to partner with *Npas4*, downstream of Ca^{2+} signaling in response to neuronal activity [68]. Unsurprisingly, the Npas-family members *Npas1/3/4* are also downregulated in discrete MGE subtypes.

Impaired NMDAR signaling alters region-specific MGE subtype marker expression

Several GABAergic/MGE markers were mis-regulated upon *Grin1*-ablation **(Figure5A)**. For example, genes *S100a0, Pthlh, Hcrtr2* that are normally expressed in SST, PV and NGFCs respectively, are upregulated in the same clusters of MGE-*Grin1*$^{fl/fl}$**(Figure5B$_i$)**, indicating a misexpression in a subtype-specific manner. Next, while certain genes such as *Reln, Tenm1* are broadly downregulated across MGE classes, some genes like *Thsd7a* show an upregulation in certain classes but a down regulation in

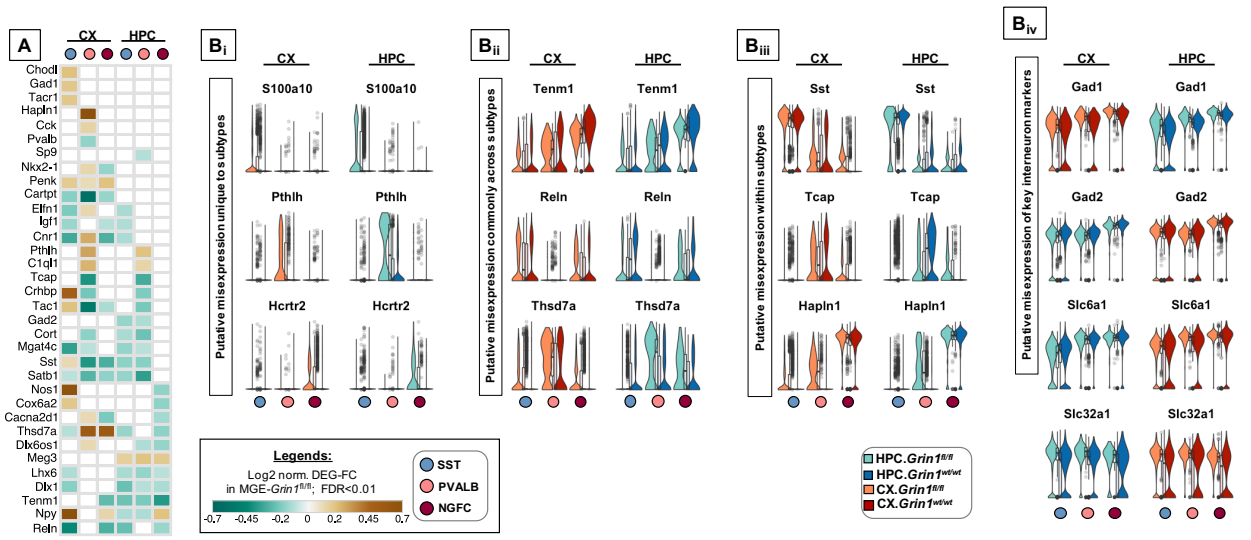

Figure 5: **Fig. 5 | Differential expression of interneuron marker genes across subtypes upon *Grin1*-ablation** A, Heatmap of log2 FC of significant DEGs in cortical and hippocampal MGE cardinal subtypes, showing a subset notable MGE marker genes. Representative box-violin plots of top differentially expressed genes from the above that represent B_i, a misexpression unique to a single MGE-*Grin1*$^{fl/fl}$ subtype; B_{ii}, a misexpression across all MGE-*Grin1*$^{fl/fl}$ subtypes; B_{iii}, a misexpression between MGE-*Grin1*$^{fl/fl}$ subtypes. B_{iv}, Representative box-violin plots of fundamental interneuron markers.

the other classes **(Figure5B$_{ii}$)**. Interestingly, a few genes that are normally abundant in one MGE class, appear to be misexpressed in another MGE class where they are not abundant. For instance, *Tcap*, that is normally expressed in PV cells, in addition to being decreased in PV cells, is upregulated in NGFCs in both cortex and hippocampus. Similarly, *Hapln1* expression which is typically limited to NGFCs, is upregulated in PV subsets **(Figure5B$_{iii}$)**. Lastly, we observed an upregulation in the *Gad1* and *Slc32a1* (vesicular GABA transporter, vGAT) and a downregulation in *Gad2* and *Slc6a1* (Na^+-Cl^-dependent GABA transporter, GAT1), corresponding with GABA synthesis and reuptake machineries respectively **(Figure5B$_{iv}$)**. Taken together, these data indicate that *Grin1*-ablation alters region-specific MGE subtype numbers, and subtype marker expression indicative of altered subtype identities.

NMDAR signaling regulates MGE subtype-specific expression of neurodevelopmental disorder risk genes

Interneuron-centric disease etiology is an emerging centrality in multiple psychiatric disorders [23]. Thus, we questioned whether the *Grin1* ablation induced DEGs presently identified correlate with disease etiology. Disease-ontology based Ingenuity Pathway Analysis of the DEGs showed significant over-representation of genes implicated in 'Schizophrenia', 'Psychiatric disorders' and 'Movement disorders', among other cellular impairments involving aberrant morphology of neurons **(Figure6A, Supplemental Table4)**. To independently examine the DEGs for potential enrichment for neurodevelopmental disorders, we obtained the risk genes for schizophrenia (Sz) and autism spectrum (As) from the SZDB [69] and SFARI [70] databases respectively. These databases curate and rank disease-relevant gene

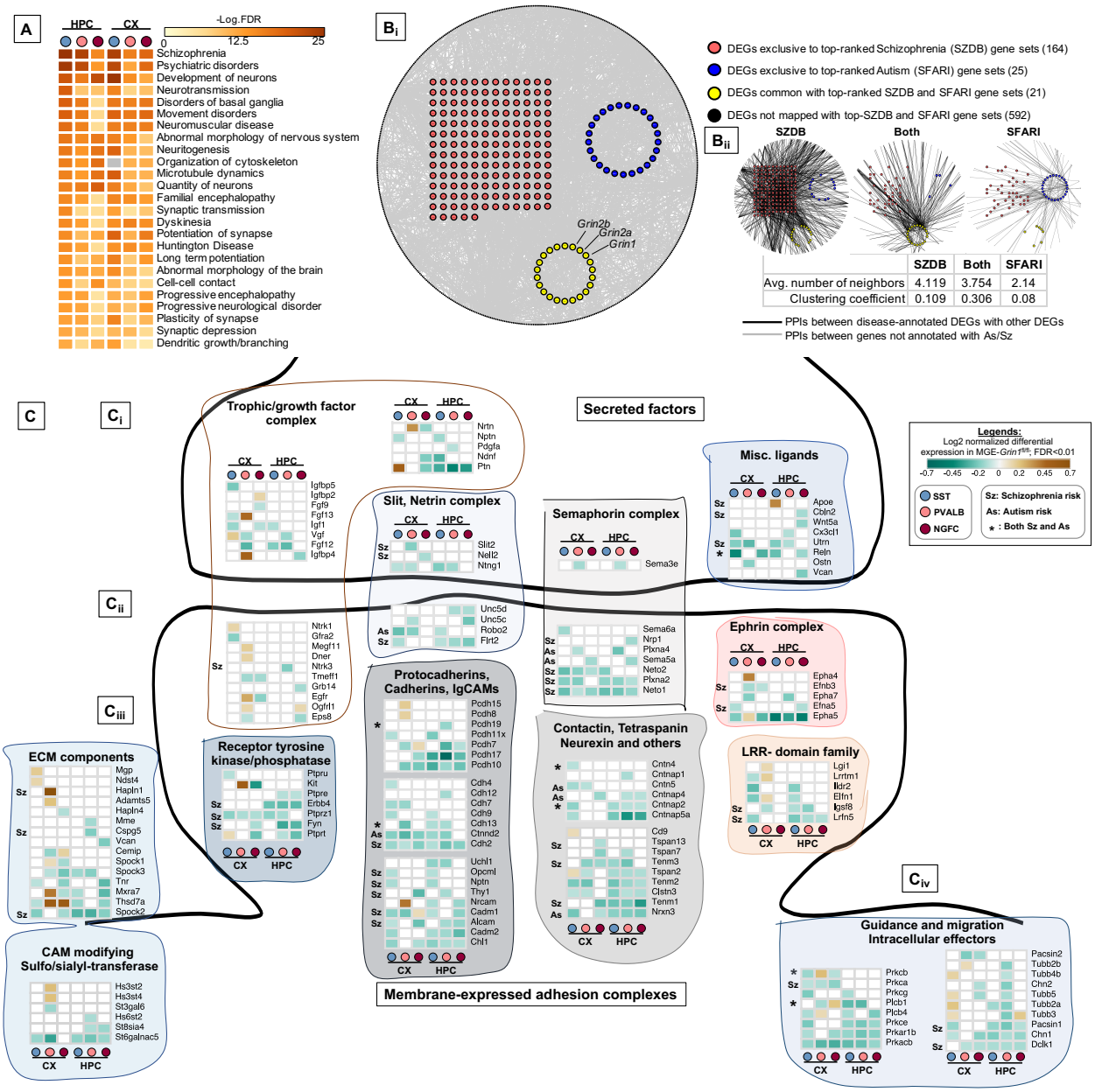

Figure 6: **Aberrant *Grin1*-signaling result in misexpression of high-risk Sz genes A,** Ingenuity Pathway Analysis of significantly overrepresented disease pathways in each MGE-subtype. $\mathbf{B}_{i,}$ Global protein-protein interaction (PPI)map among all differentially expressed genes (DEGs). Red circles indicate the DEGs annotated to be top-ranked Sz-risk genes; Blue circles indicate the DEGs annotated to be top-ranked As-risk genes; Yellow circles indicate the DEGs annotated with both Sz and As-risk genes. Black circles in the periphery indicate the DEGs not annotated with high-risk Sz/As genes. The PPIs between DEGs indicated in grey lines. $\mathbf{B}_{ii,}$ PPIs between Sz / As / dually enriched clusters, and other genes. The PPIs between disease-annotated DEGs and other disease-annotated DEGs or with other non-annotated DEGs are indicated in black lines. ThePPI between non-annotated DEGs indicated in grey lines. **C,** Heatmap of log2 FC of significant DEGs in cortical and hippocampal MGE cardinal subtypes, showing a subset of $\mathbf{C}_{i}$, secreted trophic factors and secreted ligands and guidance cues. $\mathbf{C}_{ii}$, membrane-bound synaptogenic receptors and cell adhesion molecules (CAMs) $\mathbf{C}_{iii}$, Extracellular Matrix (ECM) components and matrix modifying enzymes. $\mathbf{C}_{iv}$, Intracellular effectors of guidance and synaptogenic cues.

sets, based on multiple evidence sources including genome-wide association studies, copy-number variations, known human mutations and other integrative analyses. In particular, we mapped the DEGs with the top-ranked genes from these disease datasets (see methods for details). While 592 DEGs could not be mapped with either disease genes, 25 genes mapped exclusively with the SFARI-AS gene list, 164 genes mapped exclusively with the SZDB-Sz gene list and 21 genes mapped with both datasets **(Figure6B$_{i}$, Supplemental Table5)**. It is now well-established that several neurodevelopmental disorders exhibit a high degree of converging molecular pathways employing proteins that exist in physical complexes [71–74]. Therefore, we examined whether these disease-associated DEGs are known to form protein complexes between each other, by mapping curated protein-protein interaction (PPI) datasets for all 802 DEG products. Indeed, we observed that >95% of disease-annotated DEG products are known to exist with PPIs, while only ~75% of DEG products not annotated with Sz/As are known to exist with PPIs **(Supplemental Table5C)**. Interestingly, despite not mapping directly with the high-ranked disease gene sets, the remaining 592 genes are observed to exist in tightly-knit PPIs with the disease annotated genes. However, the PPIs mapped with SZDB form the most interconnected clusters in comparison to the SFARI-mapped PPI network **(Figure6B$_{ii}$)**, as indicated by relatively higher clustering coefficient. This indicate that members of the DEGs here identified share physical, and functional pathways in MGE-derived interneurons, contributing towards disease etiology.

Among the 210 DEGs mapped with to Sz and As, 45 genes are established regulators of axon path-finding, synapse formation and assembly, while 38 members are established regulators of membrane excitability and neuronal firing. Because both of these gene classes are intimately associated with interneuron function, we examined these classes in detail. We observed multiple classes of secreted ligands and cognate receptor families corresponding to semaphorin, netrin, slit, chemokine and growth factors, and their intracellular effectors that are downregulated upon MGE-*Grin1*-ablation **(Figure6C$_{i,iv}$)**. These include *Ntng1, Sema3e, Slit2, Cx3cl1,* and some of their receptors, *Unc5c, Nrp1, Neto1/2, Robo2* that are decreased in a MGE-class-specific manner. We observed *Fgf13* that was recently demonstrated to mediate MGE-subtype specific synapse assembly [75], to be upregulated in cortical PV cells, but downregulated in cortical SST, while *Apoe* to be upregulated in hippocampal SST cells. In addition to synaptic assembly molecules, we observed DE in a variety of synaptic adhesion molecules, corresponding to protocadherin, cadherin, ephrin and contactin families **(Figure6C$_{ii}$)**. Notably, we also observed a downregulation of *Erbb4* across all hippocampal MGE-subtypes. Lastly, we observed increased expression of extracellular matrix components *Mgp, Ndst4, Hapln1, Adamts5, Mxra7, Thsd7a* and the matrix modifying enzymes *Hs3st2/4* in cortical SST/PV subtypes **(Figure6C$_{iii}$)**.

Among the regulators of neuronal excitability, we observed a downregulation of multiple members of postsynaptic glutamate receptor subunits, GABA receptors and their associated partners **(Figure6-Supplement1B$_{ii}$)**. Interestingly, while we noted a broad downregulation of several members of potassium and sodium channel subunits, a few discrete members of the *Kcn*-families were upregulated in cortical PV and NGFC subtypes. Finally, we also observed multiple members of presynaptic GABA synthesis, release and uptake machineries including *Gad1, Syt2/10,* and *Slc6a1* differentially expressed in discrete MGE

subtypes **(Figure6, Supplement1B$_i$)**. Collectively, these findings highlight the centrality of MGE-expressed *Grin1*-signaling during synapse formation and connectivity, which when aberrantly expressed, can lead to neurodevelopmental disorders.

Discussion

Centrality of MGE-derived interneuron-expressed NMDARs from juvenile brain

NMDARs serve as critical activity dependent signaling hubs for myriad neuronal functions due to their innate ability to directly link network dynamics to cellular calcium events, and associated transcriptional coupling. Such NMDAR-dependent excitation-transcription coupling is widely established in glutamatergic neurons [76], and in specific interneurons using candidate approaches [77] within mature circuits. However, the detailed unbiased evaluation of the transcriptional landscape of NMDAR signaling within interneurons in developing circuits undergoing refinement is lacking. Our study provides the first systematic "fingerprinting" of the transcriptional coupling associated with NMDAR signaling, exclusive to MGE-derived interneurons, providing a road map for examining NMDAR regulation of MGE-derived interneurons in a subtype specific manner.

Our unbiased transcriptional profiling approach indicates that developmental NMDAR signaling participates in MGE-derived interneuron specification by regulating the expression of transcription factors (67 genes), synaptogenic (53 genes) and connectivity factors/adhesion molecules (61 genes), and regulators of membrane excitability (78 genes), among the 802 DEGs in interneurons **(Figure7)**. We employed bioinformatic analyses to examine whether system-wide downregulation of target genes can be attributed to transcription-repression elements. Indeed, we identify a set of 10 transcriptional regulators that commonly recognize the DNA-motifs present in the identified DEGs, including the master-repressor *Rest*. Future studies are needed to examine the role of these putative repressor and repression motifs that have not been previously associated with MGE-specific transcription. However, based on broad transcriptional downregulation of target genes, we can make several predictions that should guide future investigations.

Shaping interneuron identity and granularity amongst subtypes

Interneuron development from MGE is replete with combinatorial expressions of numerous transcription factors, leading to diversity [78, 79]. Several transcription factors that are impacted by Grin1-signaling are established regulators of MGE fate, subtype abundances and identities (34 genes) including *Nkx2-1, Lhx6, Dlx1, Dlx6, Maf, Mafb, Mef2c, Etv1, Npas1, Npas3* and *Sp9* [34, 56, 80–83] [84]. While the scRNAseq landscapes of interneurons predict several transcriptomic features that would classify them as distinct 'cell-types' or cell-states' [49, 85, 86] [50] the precise mechanisms responsible for such granularity is still emerging [2]. It is possible that NMDAR signaling in the developing interneuron progenitors may provide a combinatorial cue that will couple with innate genetic programs to generate the diversity in interneuron subtypes. Indicating that the *Grin1*-lacking MGE-derived interneurons have impaired subtype identities, we observe differential recoveries of the subtypes within SST, PV and NGFC in the scRNAseq assay **(Figure2-Supplement2A,B,C)**.

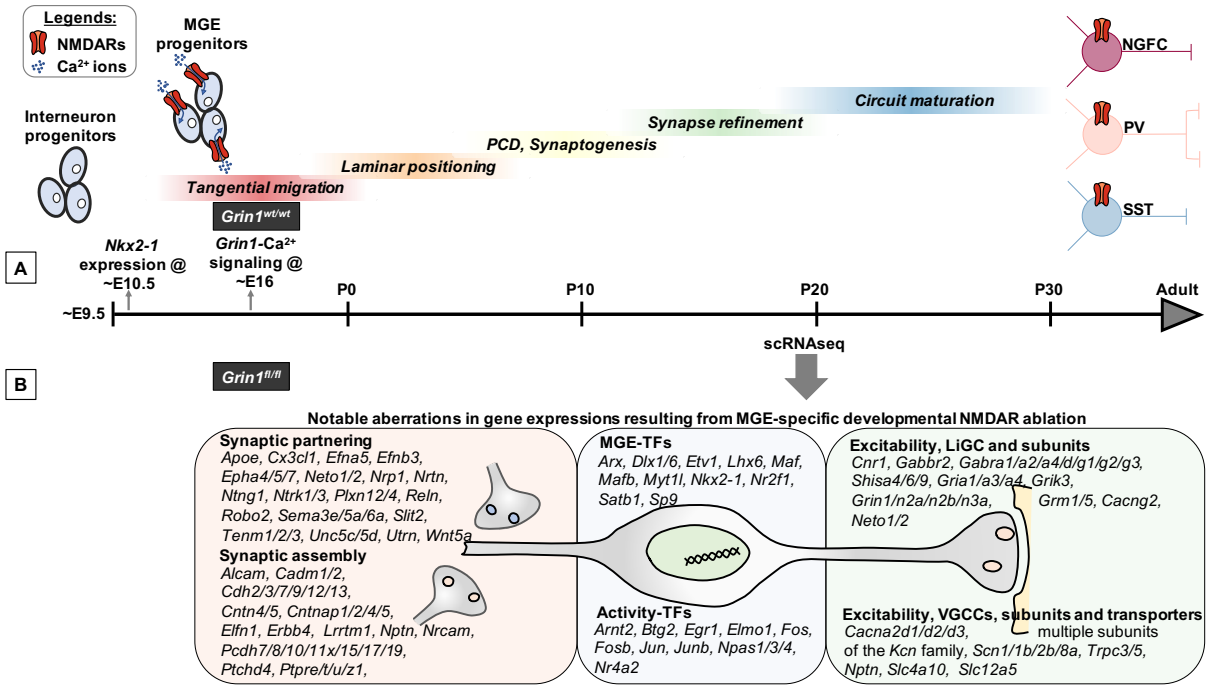

Figure 7: **Transcriptional control of MGE development, synaptic partnering and excitablity are mediated by NMDAR signaling A,** *Nkx2.1* expression appears at ~ED10.5, driving MGE subtype fate in interneuronal progenitors [42] [56]. Subsequently, their sequential developmental milestones towards circuit refinement appears to be under a combination of innate genetic mechanisms and neuronal activity. While the earliest *Grin1* expression is reported at ~ED14 in developing brain [58] [57] , MGE-specific *Grin1*-mediated Ca^{2+} is recorded at ~ED16 [15]. However, the broad role played by interneuron-expressed NMDAR signaling during interneuron development until now is not well delineated. **B,** By driving *Grin1*-ablation using *Nkx2.1*-driven Cre-recombinase, we report the earliest developmental loss of NMDAR signaling, across MGE-derived interneuron subtypes. In particular, by performing scRNAseq assay in MGE-derived interneurons from the cortex and hippocampus of the mouse brain, we report a broad transcriptional aberration subsequent to loss of NMDAR-signaling. Notably, this expression abnormality involves numerous transcriptional factors, synaptogenic and regulators of interneuron excitability, that collectively estabish MGE subtype identities.
ED, Embryonic day; PD, Postnatal day; PCD, Programmed cell death; LiGC, Ligand-gated channel; VGCC, Voltage-gated calcium channel

Particularly, we find in the *Grin1*-ablated MGE-derived interneurons, the presence of diversified PVALB.3 populations that express marker genes such as *Prox1*, otherwise not robust in our scRNAseq screen from the MGE-$Grin1^{wt}$. Additionally, by independent immunostaining experiments, we observe a modest increase in cortical SST cell numbers along with a modest decrease in cortical PV cells, in a manner similar to *Maf:Mafb*-mutants recently reported [82]. However, detailed future studies are necessary to uncover whether/how the NMDAR-dependent combinatorial transcriptional code works with innate mechanisms to generate the diversity within PV/SST/NGFC subclasses. It would be intriguing to examine whether these MGE-*Grin1*-null mice exhibit aberrations in the expression of these master MGE-regulators such as *Nkx2-1* and *Lhx6* earlier in development.

Shaping interneuron subtype-specific synaptic assembly and connectivity

What is the biological context of differential expression of the TFs, in the juvenile forebrain when MGE-derived interneuron fate is assumed to be already sealed, and subtype identities established? It is emerging that some of these TFs are continually required for the maintenance of MGE fate, post development [87]. One of the ways the TFs maintain MGE subtype fate into adulthood, is by controlling the expression of genes that are essential for ongoing interneuron function. Accordingly, we predict that NMDAR-dependent expression of synaptogenic and synaptic partnering molecules regulate the assembly of synapses with appropriate targets. Secreted semaphorin, ephrin, slit, netrin and neurotrophin-based signaling systems have been investigated in GABAergic neurons, during axonal pathfinding, and cell migration [88–95]. However, only recently have inroads been made into delineating their expression, and interaction with appropriate receptor systems in target synapses during accurate synaptogenesis. In addition, the NMDAR-dependent expression of synaptic adhesion molecules will further promote stability of newly formed synapses. Here, the mis-expression of diverse secreted cues, their receptors and adhesion molecules by MGE subtypes during *Grin1*-ablation, provides unique insight into the molecular diversity employed during synapse establishment. Our findings also reveal numerous candidates for examining subtype specific synapse assembly, which are centrally regulated by NMDAR signaling. Of particular interest are the family of protocadherins that are reported recently to be commonly downregulated in cortical interneurons generated from Sz patient-derived induced pluripotent stem cells [96].

Subsequent to synapse formation nascent connections remain susceptible to strength modifications according to neuronal activity. Again, NMDAR-signaling in MGE-derived interneurons seems to regulate this process by the transcriptional regulation of the expressions of both presynaptic and postsynaptic members, including excitatory and inhibitory synaptic molecules and their auxiliary subunits, as well as presynaptic GABA release machinery molecules such as *Cplx1/2, Stx1b, Rab3c*. However, most dramatic is the massive down regulation of several members of the potassium channel subunits and their auxiliary subunits across MGE subtypes, with the exception of an upregulation of a few *Kcn*-genes in cortical PVs and NGFCs. While the precise impact of the diverse changes in these genes on MGE firing are currently unclear, the pattern of expression of the activity-dependent transcription factors provides us an indication.

Notable activity-dependent TFs such as *Jun, Egr1* are downregulated across all MGE subtypes, while *Fosb, Fos, Arx* are down regulated across all hippocampal MGEs, and Satb1, *Arnt2* are downregulated across all cortical MGEs. In addition, *Npas4*, an established early-response TF [97–99] activated upon neuronal activity and Ca^{2+} influx in MGE-derived interneurons [100], was downregulated in cortical NGFCs upon *Grin1*-ablation. *Etv1* was previously demonstrated to be an activity-dependent TF that inversely correlates Ca^{2+} influx, regulating the identity of a subset of PV-interneurons [80]. Remarkably, we observe an increase in *Etv1* expression in cortical PV cells. Lastly, *Ostn* was recently established as an activity-regulated secreted factor [101], and we observed *Ostn* to be downregulated specifically in cortical PV subtypes (**Figure4C** $_{ii}$). Together, these changes are consistent with reduced neuronal activity in MGE subtypes upon *Grin1*-ablation, consistent with previous

reports indicating that NMDAR-antagonists can directly reduce the activity of GABAergic interneurons in adult mice [27]. Interpreting the differential expressions of activity-dependent genes during scRNAseq has been challenging, particularly, when these genes could get activated by the very process involved in cell dissociation and sorting [102, 103]. However, our use of activity-blockers and actinomycin-D throughout our MGE-$Grin1^{wt}$ and MGE-$Grin1^{fl/fl}$ scRNAseq pipelines [46], gives confidence that the differential expressions of activity-dependent TFs reflect biological relevance.

NMDAR signaling in NGFCs

Among the MGE subtypes, the PV and SST interneurons are traditionally widely studied in comparison to the dendrite-targeting NGFC subtypes (that include the Ivy cells). In the present study we provide the first detailed molecular insight into the cortical and hippocampal NGFCs, subsequent to NMDAR ablation. We anticipated that these cell types could be particularly susceptible to loss of NMDARs, since we previously reported that NGFCs exhibit the most robust synaptic NMDAR conductances among the MGE subtypes [12]. Intriguingly, while the cortical NGFCs had comparable numbers of both total and unique DEGs with respect to other cortical MGE-derived interneurons **(Figure3B)**, we observed far fewer total and NGFC-specific DEGs in the hippocampus, compared to other hippocampal MGEs. However, based on the scRNAseq cell type recoveries, we predict an elaboration of NGFC.1, and a reduction in the NGFC.2 subtype upon *Grin1*-ablation. Finally, NGFCs exhibited dendritic arborization impairments subsequent to impaired NMDAR signaling [9, 11]. Indeed, we observe 49 genes among the DEGs **(Supplemental Table1)** that have established roles in regulating neuronal cytoskeleton and associated signaling, likely mediating the observed dendritic impairments in NGFCs.

Developmental NMDAR ablation in interneurons and schizophrenia

Impaired NMDAR function observed during human NMDAR gene mutations [104], and anti-NMDAR-encephalitis [105] results in a wide range of neuropsychiatric disorders including autism spectrum disorders [106, 107], intellectual disability [108], psychosis [109], epilepsy and associated comorbidities [110, 111]. While broadly aberrant NMDAR signaling in neurons is thought to underlie a wide range of these neurological disorders, an interneuron-centric developmental NMDAR aberration is emerging central to schizophrenia-related syndromes. Indeed, in the present study, disease mapping of the DEGs using high-ranked SZDB-Sz and SFARI-As datasets indicate that many more DEGs map with the Sz than the As database. Moreover, these disease-relevent DEGs exist in physical and functional complexes with other DEGs that are not directly mapped to the Sz database. We used only stringent, high-ranked disease genes from the database that pass several disease-relevant criteria. However, there are other DEGs that still map to lower-ranked Sz and As datasets that are 'non-annotated' in present study. While our study can be argued as an 'extreme' case of NMDAR hypofunction in MGE-derived interneurons, it provides a starting point highlighting the centrality and broad range of interneuronal NMDAR-transcriptional pathways during development.

A multitude of studies implicate NMDAR-hypofunction specific to PV cell types as a central underlying feature of schizophrenia etiology [112, 113]. However, the measurable NMDAR conductances within PV interneurons are relatively small in comparison to other MGE

subtypes [12] . Additionally, NMDA signaling in non-PV interneuron subtypes drives robust dendritic inhibition in pyramidal neurons [114, 115]. Moreover, while NMDAR-ablation in *Pvalb*-Cre lines produces other behavioral deficits unrelated to the Sz-like phenotypes [30, 33] , a developmental, but not adult-onset *Grin1*-ablation in *Ppp1r2*-Cre line [29] that targets a subset of PV interneurons among other subtypes [116], recapitulates core Sz-like phenotypes. Lastly, studies that map interneuron subtypes to Sz-like phenotypes indeed support the role of different interneuron classes beyond PV cells towards disease etiology [28, 33].

Integrating these ideas and based on findings from the present study, we propose the following: (i) Despite a smaller NMDAR conductance in PV interneurons, we observe a robust transcriptional coupling via NMDARs, as observed by several distinct gene expression abnormalities in this cell type relevant to human Sz. Therefore, PV-expressed NMDARs primarily serve to regulate transcriptional coupling, mediating the abundances of PV-subtype abundances. (ii) The developmental window for NMDAR loss of function is particularly important because, its transcriptional regulation maintains the correct synaptogenic and assembly cues, which when lost, lead to disease causing-impaired connectivity. Perhaps, in the *Grin1*$^{fl/fl}$: *Pvalb*-Cre mouse line, the *Grin1*-ablation occurs only at a developmental window when synaptic connectivity is sufficiently complete, explaining why the animal model does not lead to profound Sz-like impairments. (iii) The dendrite targeting SST and NGFC interneurons also exhibit robust NMDAR signaling and transcriptional coupling. During aberrant NMDAR-transcriptional coupling, it is therefore likely that impaired dendritic connectivity and inhibition onto pyramidal neurons also contributes towards disease etiology. Therefore, our dataset provides credence to interneuronal subtype-specific granularilty, connectivity and excitability, all playing combinatorial and mutually-supporting roles during disease etiology.

Taken together, our study presents a rich resource, laying the road map for systematic examination of NMDAR signaling in interneuron subtypes, by providing multiple molecular targets for examination in both normal and impaired circuits.

Materials and methods

Contact for Reagent and Resource Sharing

Further information and requests for resources and reagents should be directed to and reasonable requests will be fulfilled by the Lead Contact, Chris McBain (mcbainc@mail.nih.gov).

Animals

All experiments were conducted in accordance with animal protocols approved by the National Institutes of Health. The Nkx2.1-Cre driver line (C57BL/6J-Tg(*Nkx2*-1-Cre)2Sand/J; Cat. No. 008661 | Nkx2.1-Cre, Floxed Grin1 mouse line (B6.129S4-Grin1^{tm2Stl}/J; Cat. No. 005246 | fNR1) and Ai14 reporter mouse (B6.Cg-Gt (ROSA)26Sor$^{tm14(CAG-tdTomato)Hze}$/J; Cat. No. 007914 | Ai14, Ai14D or Ai14(RCL-tdT)-D), purchased from the Jackson Laboratory, were used to generate the MGE-derived interneuron-specific *Grin1*$^{fl/fl}$ line. Littermate MGE-Grin1$^{wt/wt}$controls, and both male and female mice were used during this study. Mice were housed and bred in conventional vivarium with standard laboratory chow and water in

standard animal cages under a 12hr circadian cycle. Genotyping of the mice were performed as indicated in the appropriate Jackson Laboratory mice catalog.

Single-cell dissociation and FACS

P18-20 juvenile *Nkx2*-1-Cre: Grin1$^{wt/wt}$: TdT^{+} and Nkx2-1-Cre: Grin1$^{fl/fl}$: TdT^{+} mice were used for single-cell sequencing experiments. All mice were anesthetized with isoflurane and then decapitated. Brain dissection, slicing and FACS sorting were carried out as described [43, 44], with slight modifications. NMDG-HEPES–based solution was used in all steps to enable better recovery of the cells [45] during FACS sorting and single-cell bar coding. Briefly, the brain sectioning solution contained NMDG-HEPES–based high-Mg^{2+} cutting solution contained 93 mM NMDG, 2.5 mM KCl, 1.2 mM NaH_2PO_4, 30 mM $NaHCO_3$, 20 mM HEPES, 25 mM glucose, 5 mM sodium ascorbate, 3 mM sodium pyruvate, 2mM Thiourea, 10 mM $MgSO_4$*$7H_2O$, and 0.5 mM $CaCl_2$*$2H_2O$; it was adjusted to pH 7.4 with 12.1N HCl, an osmolarity of 300-310 mOsm, and carbogenated (mix of 95% O_2 and 5% CO_2) before use. This solution was chilled and the process of sectioning were conducted on a ice-chamber in the vibratome.

3-4, *Nkx2-1*-Cre: *Grin1*$^{wt/wt}$: TdT^{+} or *Nkx2-1*-Cre: *Grin1*$^{fl/fl}$: TdT^{+} mice were processed on consecutive days for single-cell sequencing experiments. TdT negative animals were processed in parallel for initially setting FACS gate for the Tomato-channel. Across the replicates, 10XMGE-Grin1-WT and 6XMGE-Grin1-null animals were used for the scRNAseq. Coronal slices containing frontal cortex and hippocampus (350mM) were cut using VT-1000S vibratome (Leica Microsystems) in cold NMDG-HEPES–based high-Mg^{2+} cutting solution. Slices were recovered in the same solution at 20°C for 30 minutes during when, they were visually inspected under fluorescence microscope and micro dissected, all under constant carbogenation. The recovery and microdissection were conducted in the NMDG-HEPES high-Mg^{2+} solution supplemented with 0.5μM tetrodotoxin (TTX), 50 μM DL -2-Amino-5-phosphonopentanoic acid (APV) and 10 μM Actinomycin-D (Act-D).

Cell dissociation was performed using the Worthington Papain Dissociation System (LK003150) according to manufacturer instructions with minor modifications. Briefly, single-cell suspensions of the micro dissected frontal cortices or hippocampus were prepared using sufficiently carbogenated dissociation solution (containing Papain, DNAse in Earle's Balanced Salt Solution, EBSS), supplemented with 1μM TTX, 100 μM APV and 20 μM Act-D. After a 60 min enzymatic digestion at 37°C, followed by gentle manual trituration with fire-polished Pasteur pipettes, the cell dissociates were centrifuged at 300g for 5 minutes at 20°C, and the supernatants were discarded. The enzymatic digestion was quenched in the next step by the addition of ovomucoid protease inhibitor. Albumin density gradient was performed on the pellets, using a sufficiently carbogenated debris removal solution (containing albumin-ovomucoid inhibitor, DNAse in EBSS). The resulting cell pellets were resuspended in 1ml FACS buffer containing 10% FBS, 10U/μl of DNAse, 1μM TTX, 100 μM APV and 20 μM Act-D in a 50:50 mix of carbogenated EBSS: NMDG-HEPES–based cutting saline (with 1mM $MgSO_4$*$7H_2O$, it is important to not use High-Mg^{2+} in the FACS buffer, as it interferes with the subsequent 10X scRNAseq reaction). Cells were placed in polystyrene tubes (Falcon 352235) on ice during the FACS.

For single cell sorting of TdT^{+} expressing cells by FACS, resuspended cell dissociates

were filtered through 35mm cell strainer (Falcon 352235) to remove cell clumps. The single cell suspensions were then incubated with 1mg/ml DAPI (1:500, Thermo Scientific 62248) and 1mM DRAQ5 (Thermo Scientific 62251) at 4°C for 5 minutes to label dead cells and live cells respectively. Samples were analyzed for TdTomato expression and sorted using a MoFlo Astrios EQ high speed cell sorter (Beckman Coulter). TdT-negative cells were used as a control to set the thresholding FACS gate for the detection and sorting of the Ai14-TdTomato-expressing cells, and the same gate was then applied for all subsequent experiments. Flow data analysis and setting of sorting gates on live (DAPI-negative, DRAQ5-positive) and Ai14-TdTomato-expressing cells were carried out using Summit software V6.3.016900 (Beckman Coulter). Per sample/session, 20,000 – 40,000 individual cells were sorted into a FBS-precoated, Eppendorf LoBind Microcentrifuge tubes containing carbogenated 10ml FACS buffer, that served as the starting material for 10X Genomics bar-coding.

10X Genomics Chromium

The cells were inspected for viability, counted, and loaded on the 10X Genomics Chromium system, aiming to recover ~5000 cells per condition. 12 PCR cycles were conducted for cDNA amplification, and the subsequent library preparation and sequencing were carried out in accordance with the manufacturer recommendation (Chromium^{TM} Single Cell 3' Library & Gel Bead Kit v2 and v3, 16 reactions). Sequencing of the libraries were performed on the Illumina HiSeq2500 at the NICHD, Molecular Genomics Core facility. Replicate 1 of the scRNAseq were performed using 10X v2 reaction from which, the cell estimates, mean reads per cell (raw), median genes per cell respectively, are as follows Cortical WT: 1277, 149K, 4615; Cortical NULL: 181, 159K, 4826; Hippocampal WT: 2221, 92K, 2578; Hippocampal NULL: 404, 154K, 4903. Replicate 2 of the scRNAseq were performed using 10X v3 reaction from which, the cell estimates, mean reads per cell (raw), median genes per cell respectively, are as follows Cortical WT: 3851, 22.8K, 1536; Cortical NULL: 2898, 23.5K, 2759; Hippocampal WT: 4600, 23.6K, 850; Hippocampal NULL: 4436, 25.8K, 3143. Replicate 3 of the scRNAseq were performed using 10X v3 reaction from which, cell estimates, mean reads per cell (raw), median genes per cell respectively, are as follows Cortical WT: 3960, 24.8K, 2870; Hippocampal WT: 3159, 26.9K, 2956. Representative quality metrics from Replicate 2 are indicated in **Figure1-Supplement1B,C ,D,E.** Demultiplexed samples were aligned to the mouse reference genome (mm10). The end definitions of genes were extended 4k bp downstream (or halfway to the next feature if closer), and converted to mRNA counts using the Cell Ranger Version 2.1.1, provided by the manufacturer.

Data processing, analyses, visualization and differential expression testing

Processing (load, align, merge, cluster, differential expression testing) and visualization of the scRNAseq datasets were performed with the R statistical programming environment [117] (v3.5.1) and Seurat package (v3.1.5, a development version of Seurat v3.1.5.9000 was used to generate violin plots in 2C and 5B) [47, 48] . Data set preprocessing, comparison of WT- and NULL-Ai14 cells, canonical correlation analyses, and differential expression of genes ($p_{adj} < 0.01$) within the same cluster between WT- and NULL-Ai14 cells were performed according to default Seurat parameters, unless otherwise mentioned. Quality control filtering was performed by only including cells that had between 200-6000 unique genes, and that had <30% of reads from mitochondrial genes. While the WT replicates

had no cells above 30% mitochondrial genes, only NULL replicates from both brain regions exhibited 7-12% of cells above this threshold. Suggestive of inherent biological impact of *Grin1*-ablation, we repeated the clustering and subsequent analyses without excluding any cells. These analyses did not alter the clustering or skew the gene list. Clustering was performed on the top 25 PCs using the function FindClusters() by applying the shared nearest neighbor modularity optimization with varying clustering resolution. A cluster resolution of 1.0 was determined to be biologically meaningful, that yielded all known MGE cardinal classes. Initial analyses were performed on the WT datasets separately (WT.alone), and similar set of analysis parameters were applied when the WT and NULL samples were merged (WT.NULL.integrated) for subsequent differential expression testing. Phylogenetic tree relating the 'average' cell from each identity class based on a distance matrix constructed in gene expression space using the BuildClusterTree() function. Overall, we identified 27, and 33 clusters using this approach in the WT.alone, and WT.NULL.integrated assays respectively. The WT.alone correspond to 11 MGE.GAD1/2 clusters **(Figure1&2)**, while the WT.NULL.integrated assay correspond to 12 clusters **(Figure5-Supplement.1).** We first searched for the top differential markers for each MGE subcluster using the FindAllMarkers() function. The genes thus identified for the integrated data is presented in ***Supplemental Table1b***. Determination of MGE and non-MGE identities are performed based on existing interneuron literature and other scRNAseq datasets [1, 43, 50, 53, 85, 87, 118–120]. The labels from Figures 1 and 2 are matched with the top gene markers identified by the FindAllMarkers() function and the similarly named clusters in Figures 1 and 2 have the same identities. Lastly, for the integrated analyses and differential expression testing, we first merged the identities of the subclusters SST.1-SST.6 and TH.1, and relabelled as SST subset; PVALB.1-3 relabelled as PVALB subset; and NGFC.1-2 relabelled as the NGFC subset during subsequent analysis **(Figure3)**.

Differential gene expression testing were performed using the MAST package within the FindMarkers function to identify the differentially expressed genes between two subclusters. MAST utilizes a hurdle model with normalized UMI as covariate to generate the differential fold changes [121] , and is known to result in underestimation of the magnitude of fold change (FC) [122]. Therefore, while applying a stringent false-discovery rate <0.01, we determined the minimum FC based on the control gene *Grin1*, which is the target gene knocked out in MGE-derived interneuron celltypes. Notably for *Grin1*, we had previously demonstrated that the NGFCs which carry maximum NMDAR component among MGEs, are devoid of NMDAR current at this comparable age [9] . In the present scRNAseq assay, we observe a logFC for Grin1 ranging between -0.1 to -0.35 across both brain regions and all MGE subtypes. Therefore, we determined a minimum logFC in our DEGs as ± 0.1 to be meaningful. Previous studies have demonstrated the MAST approach for DEG testing to be powerful in determining subtle changes in highly transcribed genes, and among abundant populations, additional to under representing changes among weakly transcribed genes [121, 122] . Volcano plots and Heat maps for the DEG were generated using EnhancedVolcano package [123] and Morpheus package https://software.broadinstitute.org/morpheus within the R framework.

Pathway analyses, PPI network mapping and disease mapping

Ingenuity Pathway Analyses were conducted on the differentially expressed genes to generate the molecular functional annotation and to identify the biological pathways and disease pathways overrepresented. This tool was also used to annotate genes with their known cellular functional classes. Additional Gene Ontology mapping and KEGG analyses were conducted using ShinyGO [124]. Protein-protein interaction (PPI) mapping datasets from a variety of curated databases [125–127] were conducted as previously described [72] [128] using the Cytoscape [129] platform (v3.8.0). Schizophrenia risk genes integrated from various sources including genome-wide association studies (GWAS), copy number variation (CNV), association and linkage studies, post-mortem human brain gene expression, expression quantitative trait loci (eQTL) and encyclopedia of DNA elements (ENCODE), were downloaded from http://www.szdb.org/ [69] . Autism Spectrum Disorder risk genes integrated from various sources were downloaded from Simons Foundation https://gene.sfari.org/ [70]. SZDB genes that had a integrated total score of 3-6 (1419 genes, 22% out of 6387) were considered 'high-risk' for DEG mapping **(Supplemental Table5a)**. SFARI genes scored 1-2 with accounting for a high strength of evidence (392 genes, 42% out of 943), were considered 'high-risk' for DEG mapping **(Supplemental Table5b)**. Transcriptional factor motif enrichment search using the iRegulon [62] was also conducted using Cytoscape using default parameters.

Immunostaining

All solutions were freshly prepared and filtered using 0.22μm syringe filters for parallel treatments of wildtype and MGE-Grin1-null groups. Adult mice of postnatal day (PD) 30/60/210 were Mice were deeply anesthetized with isoflurane and perfused transcardially with 1X phosphate buffer saline (PBS) and followed by the fixative 4% paraformaldehyde. The brains were post-fixed in the same fixative for overnight at 4 °C for the immunostaining assays. Postfixed brains were serially dehydrated using 10%/20%/30% sucrose solutions at 4 °C. Coronal sections (50 μm) were cut on a freezing microtome. Immunostaining was performed on free-floating sections. Tissue sections were permeabilized and blocked in 1 × PBS + 1% bovine serum albumin + 10% normal goat serum + 0.5% Triton X-100 (Carrier PB) at room temperature for 2 h, followed by incubation in primary antibodies, listed below, diluted with 1 × PBS + 1% bovine serum albumin + 1% normal goat serum + 0.1% Triton X-100 overnight at 4 °C. Tissue sections were then incubated with secondary antibodies, listed below, diluted in Carrier Solution (1:1000), and DAPI (1:2000) at room temperature for 1–2 h and mounted on Superfrost glass slides, and coverslipped using Mowiol mounting medium and 1.5 mm cover glasses.

Antibodies

The following primary antibodies were used: mouse anti-PV (1:1000; Sigma-Aldrich Cat# P3088, RRID: AB_477329), rat anti-SST (1:1000; Millipore Cat# MAB354, RRID: AB_2255365). Secondary antibodies were conjugated with Alexa Fluor dyes 488 or 633 (1:1000; Thermo Fisher Scientific).

Image acquisition and analysis

Mouse brains from 4–8 different animals were used for each condition, and section depth were matched between the genotypes for parallel immunostaining. Fluorescent images were captured using the 10X objective of a Nikon Widefield Fluorescence, Spinning Disk Confocal

microscope. For all slices with immunostained or genetically reported signal, 50 μm thin sections were imaged using 10x/0.45 CFI PlanApo objective (imaging settings: Numerical Aperture 0.75, bit depth 16-bit, Exposure 100ms). Confocal stacks were stitched using NIS Elements (Nikon) before importing them into Imaris software (Bitplane, version 9.2). Cell bodies were marked in Imaris software using the 'Spots' function. *Nkx2-1*-Cre:TdT$^+$ RFP+, PV+ cell bodies were detected using the automatic function, with a signal detection radius of 10 μm. The Imaris 'Quality' filter was set above an empirically determined threshold to maximize the number of detected cells while minimizing observed false positives. SST+ cell bodies were marked manually using the Imaris 'Spots' function. ROI 3D borders around hippocampus or cortex, drawn manually using the Imaris function 'Surfaces'. Spots were then split within each ROI using the Imaris function 'Split Spots'. Overlap of RFP+ cells with other markers (PV, SST) was addressed by filtering the RFP+ Spots above an empirically determined threshold intensity in the channel relative to the marker of interest. Each image with an automatic analysis by Imaris was checked by an expert and incorrectly identified cell bodies where refined if required. In **Figure5A,B** Error bars reflect standard error of mean; Two-tailed unpaired t-test was performed using Prism8.

Author contributions

VM and CJM conceived the project. VM, TJP and CJM designed the experiments, DM performed FACS sorting and analysis. VM, YZ, TJP performed 10X scRNAseq. VM, AM, CJR, CE, RD performed 10X scRNAseq bioinformatic analyses. VM and AP conducted immunuflourescent staining, imaging and analysis. CJM supervised the study. VM and CJM wrote the paper and all authors edited the manuscript.

Acknowledgment

This work was supported by *Eunice Kennedy Shriver* NICHD Intramural Award to CJM. We thank Steven L. Coon, Tianwei Li and James R. Iben at the Molecular Genomics Core, NICHD, for RNA sequencing and bioinformatics support. We thank Vincent Schram and Lynne Holtzclaw of the NICHD Microscopy and Imaging Core for imaging support, and we thank Carolina Bengtsson Gonzales for assistance with improving cell viability during dissociation and FACS. We also thank Xiaoqing Yuan, Steven Hunt, Daniel Abebe for assistance with animal colony maintenance.

References

[1] K. A. Pelkey, R. Chittajallu, M. T. Craig, L. Tricoire, J. C. Wester, C. J. McBain, Hippocampal GABAergic Inhibitory Interneurons, Physiological Reviews 97 (4) (2017) 1619–1747. doi:10.1152/physrev.00007.2017.
URL https://dx.doi.org/10.1152/physrev.00007.2017

[2] B. Wamsley, G. Fishell, Genetic and activity-dependent mechanisms underlying interneuron diversity, Nature Reviews Neuroscience 18 (5) (2017) 299–309. doi:10.1038/nrn.2017.30.
URL https://dx.doi.org/10.1038/nrn.2017.30

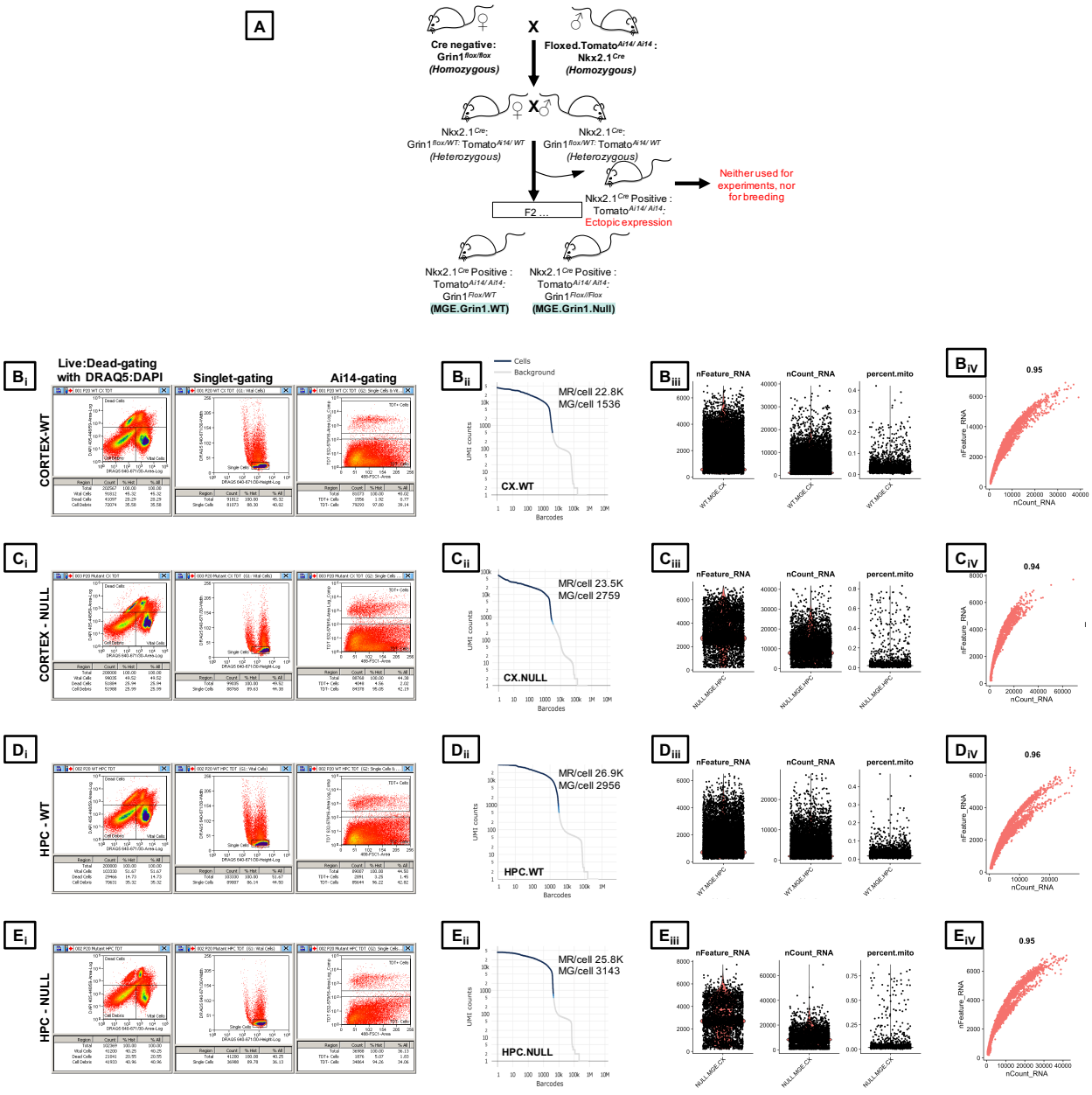

Figure 8: **(Figure1, Supp.1) | Schematic overview and quality control for scRNAseq A,** Breeding strategy, $\mathbf{B_i}$,$\mathbf{C_i}$,$\mathbf{D_i}$,$\mathbf{E_i}$, Representative FACS gates to sequentially isolate live: dead cells using DAPI: DRAQ5 staining, singlet-gating and TdT^+-reporter gating to obtain reporter-positive MGE-derived interneurons from frontal cortex and hippocampus. $\mathbf{B}_{ii}$,$\mathbf{C_{ii}}$,$\mathbf{D}_{ii}$,$\mathbf{E}_{ii}$, Barcode Rank Plots for cells from WT and NULL mice, demonstrating separation of cell-associated barcodes and those associated with empty partitions. UMI, unique molecular identifier; MR, Mean Reads; MG, Median Genes. $\mathbf{B_{iii}}$,$\mathbf{C}_{iii}$,$\mathbf{D_{iii}}$,$\mathbf{E}_{iii}$, Distributions of the total number of genes, percentage of mitochondrial genes and UMIs per cell in control mice $\mathbf{B_{iv}}$,$\mathbf{C}_{iv}$,$\mathbf{D}_{iv}$,$\mathbf{E}_{iv}$, Pearson correlation coefficient of the distributions of the total number of genes and the UMI

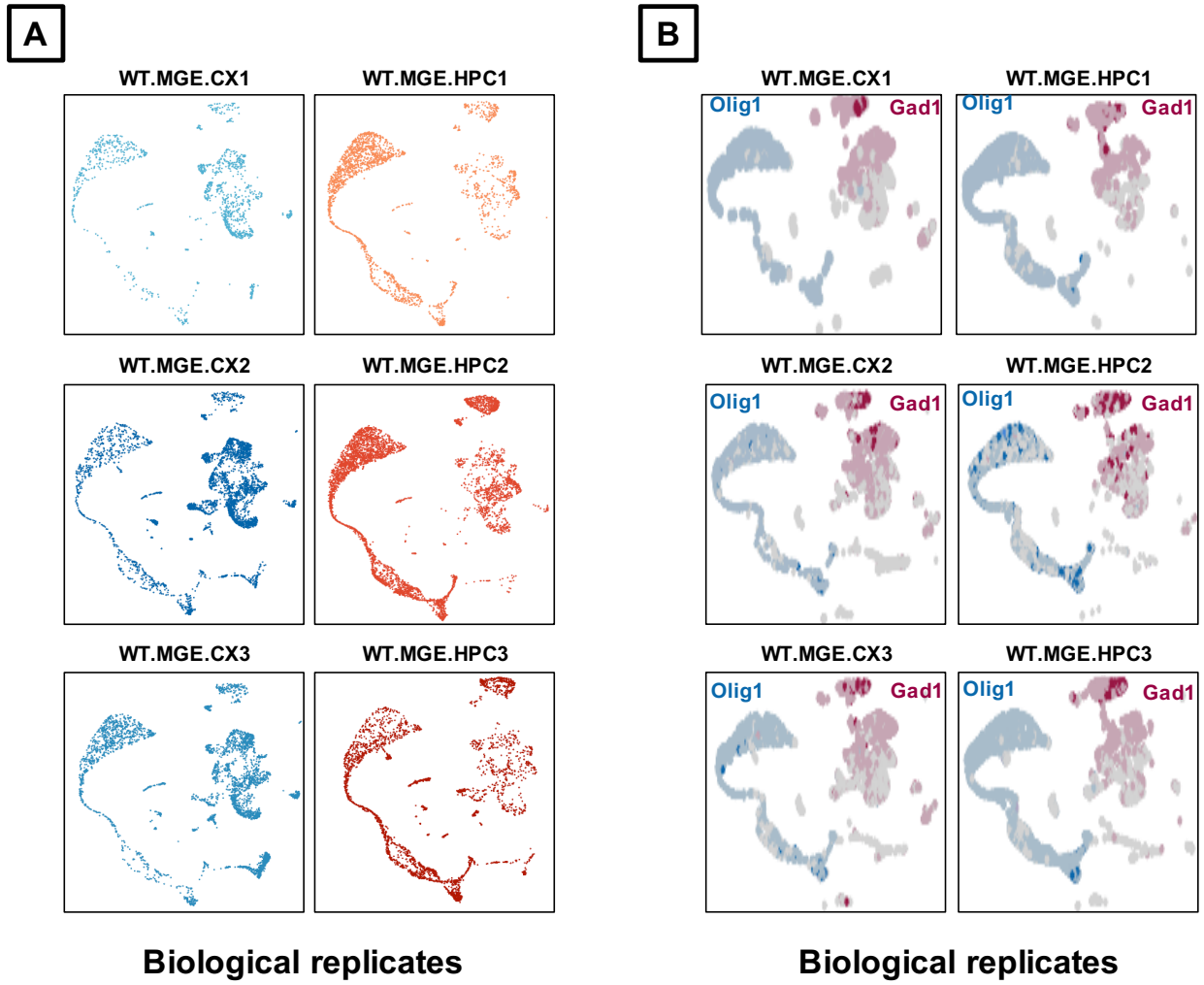

Figure 9: **(Figure1, Supp.2) | Biological replicates** Representative UMAP plots of the 3 biological replicates from cortex and hippocampus indicates **A,** similar clustering, and **B,** similar expression profiles of *Nkx2-1*-derived, *Gad1*-expressing MGE-derived interneurons and *Nkx2-1* derived, *Olig1*-expressing oligodendrocytes.

[3] L. Tricoire, K. A. Pelkey, B. E. Erkkila, B. W. Jeffries, X. Yuan, C. J. McBain, A Blueprint for the Spatiotemporal Origins of Mouse Hippocampal Interneuron Diversity, Journal of Neuroscience 31 (30) (2011) 10948–10970. doi:10.1523/jneurosci.0323-11.2011.
URL https://dx.doi.org/10.1523/jneurosci.0323-11.2011

[4] L. Tricoire, K. A. Pelkey, M. I. Daw, V. H. Sousa, G. Miyoshi, B. Jeffries, B. Cauli, G. Fishell, C. J. McBain, Common Origins of Hippocampal Ivy and Nitric Oxide Synthase Expressing Neurogliaform Cells, Journal of Neuroscience 30 (6) (2010) 2165–2176. doi:10.1523/jneurosci.5123-09.2010.
URL https://dx.doi.org/10.1523/jneurosci.5123-09.2010

[5] F. M. Krienen, M. Goldman, Q. Zhang, R. D. Rosario, M. Florio, R. Machold, A. Saunders, K. Levandowski, H. Zaniewski, B. Schuman (2019).

[6] L. Overstreet-Wadiche, C. J. McBain, Neurogliaform cells in cortical circuits, Nature Reviews Neuroscience 16 (8) (2015) 458–468. doi:10.1038/nrn3969.

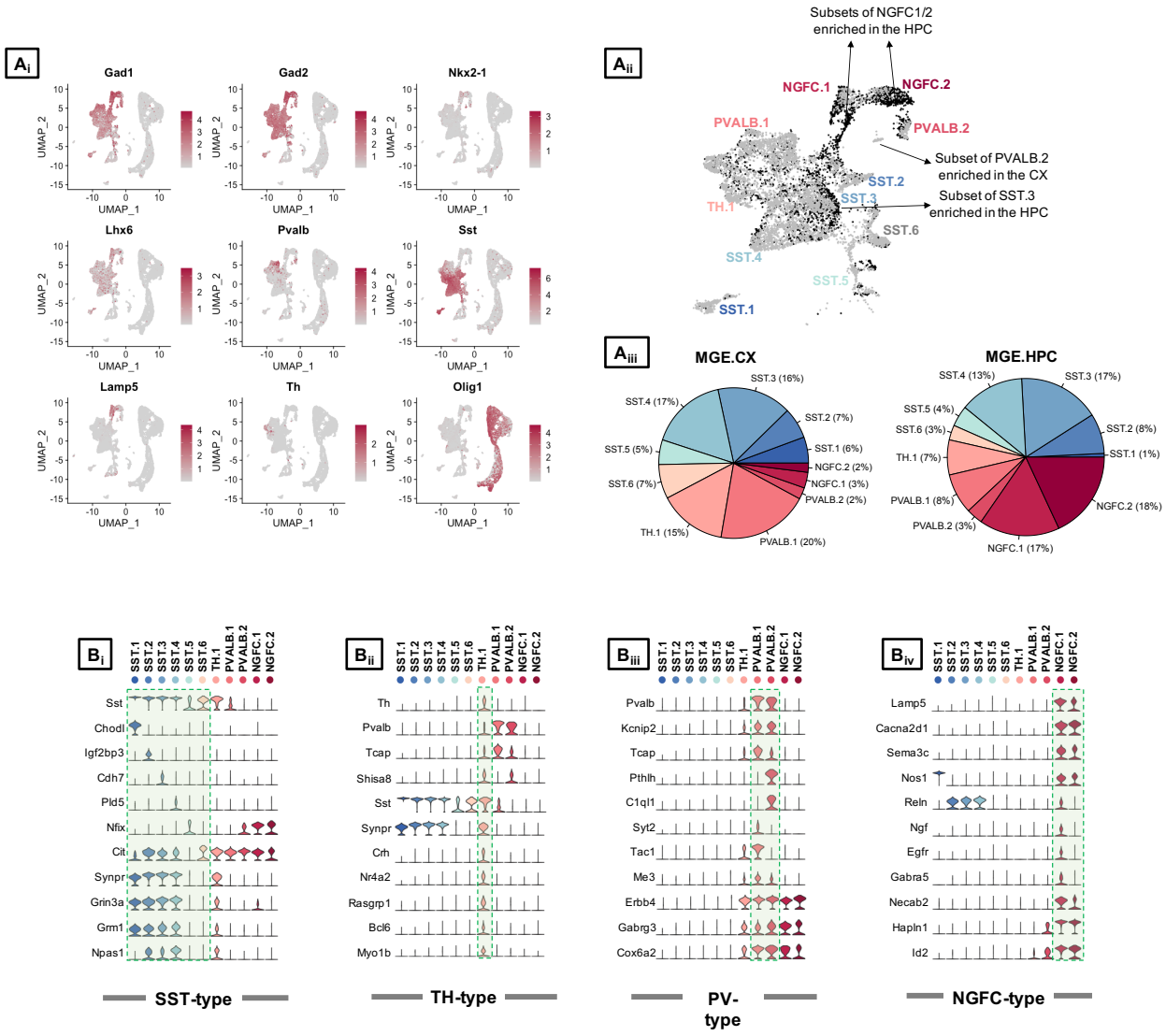

Figure 10: **(Figure1, Supp.3) | Select marker gene expression across the subtypes of merged cortical and hippocampal MGE-*Grin1*** $^{wt/wt}$ **A**$_i$, UMAP representation of cardinal MGE markers genes in the cortical and hippocampal merged dataset. **A**$_{ii}$, UMAP representation colored by region, highlighting the region-specific enrichments of MGE subsets. **A**$_{iii}$, Pie chart indicating the percentages of cells recovered across the interneuron subtypes from cortex and the hippocampus. **B**, Violin plot showing the distribution of expression levels of well-known representative cell-type-enriched marker genes across the 11 MGE subtypes.

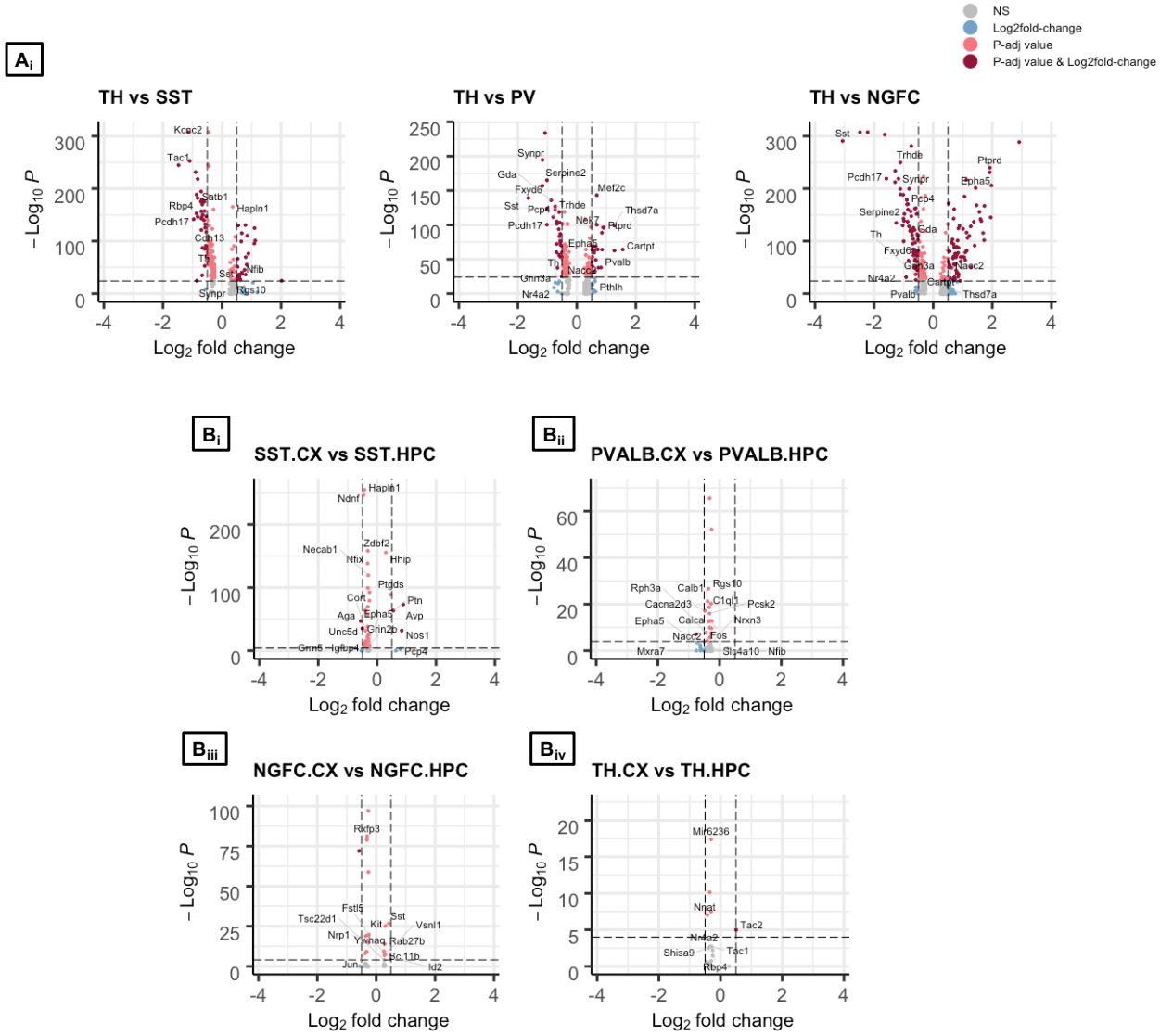

Figure 11: **(Figure1, Supp.4) | MGE subtype differences between cortex and hippocampus** Volcano plot representing the −log10 False Discovery Rate (FDR) versus log2 fold change (FC) between **A,** TH-expressing MGE subsets and the remaining MGE subset SST, PVALB and NGFC; **B,** Differential expression of the cardinal MGE classes between cortex and hippocampus, at a fold change ≥0.5 and FDR <10e-5.

URL https://dx.doi.org/10.1038/nrn3969

[7] T. Klausberger, P. Somogyi (2008).

[8] G. Akgül, C. J. McBain, Diverse roles for ionotropic glutamate receptors on inhibitory interneurons in developing and adult brain, The Journal of Physiology 594 (19) (2016) 5471–5490. doi:10.1113/jp271764.
URL https://dx.doi.org/10.1113/jp271764

[9] R. Chittajallu, J. C. Wester, M. T. Craig, E. Barksdale, X. Q. Yuan, G. Akgül, C. Fang, D. Collins, S. Hunt, K. A. Pelkey, C. J. McBain, Afferent specific role of NMDA receptors for the circuit integration

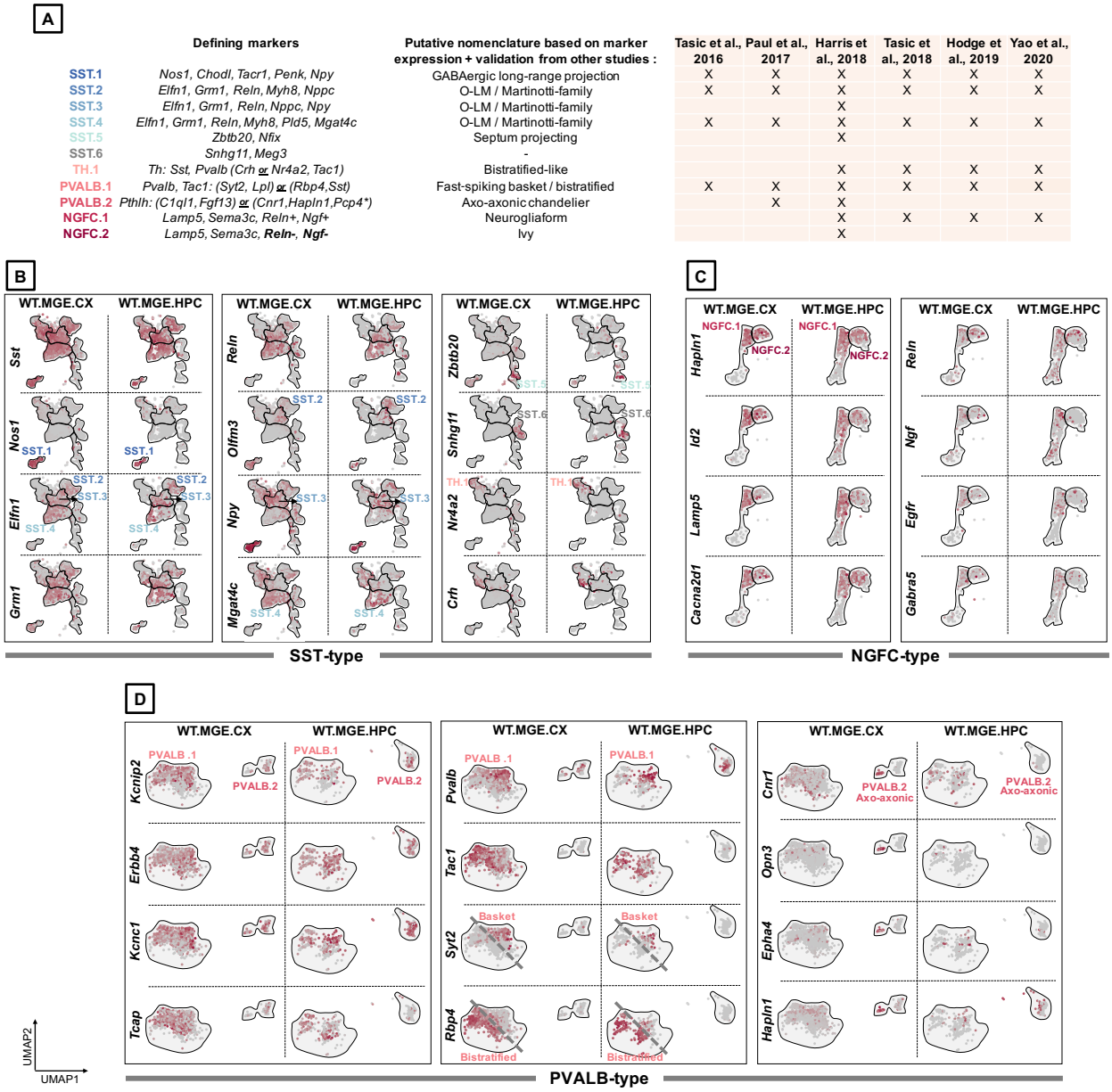

	Defining markers	Putative nomenclature based on marker expression + validation from other studies :	Tasic et al., 2016	Paul et al., 2017	Harris et al., 2018	Tasic et al., 2018	Hodge et al., 2019	Yao et al., 2020
SST.1	*Nos1, Chodl, Tacr1, Penk, Npy*	GABAergic long-range projection	X	X	X	X	X	X
SST.2	*Elfn1, Grm1, Reln, Myh8, Nppc*	O-LM / Martinotti-family	X	X	X	X	X	X
SST.3	*Elfn1, Grm1, Reln, Nppc, Npy*	O-LM / Martinotti-family			X			
SST.4	*Elfn1, Grm1, Reln, Myh8, Pld5, Mgat4c*	O-LM / Martinotti-family	X	X	X	X	X	X
SST.5	*Zbtb20, Nfix*	Septum projecting			X			
SST.6	*Snhg11, Meg3*	-						
TH.1	*Th: Sst, Pvalb (Crh or Nr4a2, Tac1)*	Bistratified-like			X	X	X	X
PVALB.1	*Pvalb, Tac1: (Syt2, Lpl) or (Rbp4,Sst)*	Fast-spiking basket / bistratified	X	X	X	X	X	X
PVALB.2	*Pthlh: (C1ql1, Fgf13) or (Cnr1,Hapln1,Pcp4*)*	Axo-axonic chandelier		X	X			
NGFC.1	*Lamp5, Sema3c, Reln+, Ngf+*	Neurogliaform			X	X	X	X
NGFC.2	*Lamp5, Sema3c, **Reln-**, **Ngf-***	Ivy			X			

Figure 12: **(Figure1, Supp.5) | MGE subtype annotation based on marker expression A,** Table indicating the subype-defining marker genes observed in the present study and their descriptions in the previous scRNAseq datasets (*indicates the genes expressed in the cortex-exclusive PVALB.2 subcluster). Representative UMAP plots of MGE subtype-enriched genes in **B,** SST subclusters, **C,** NGFC subclusters, and **D,** PVALB subclusters.

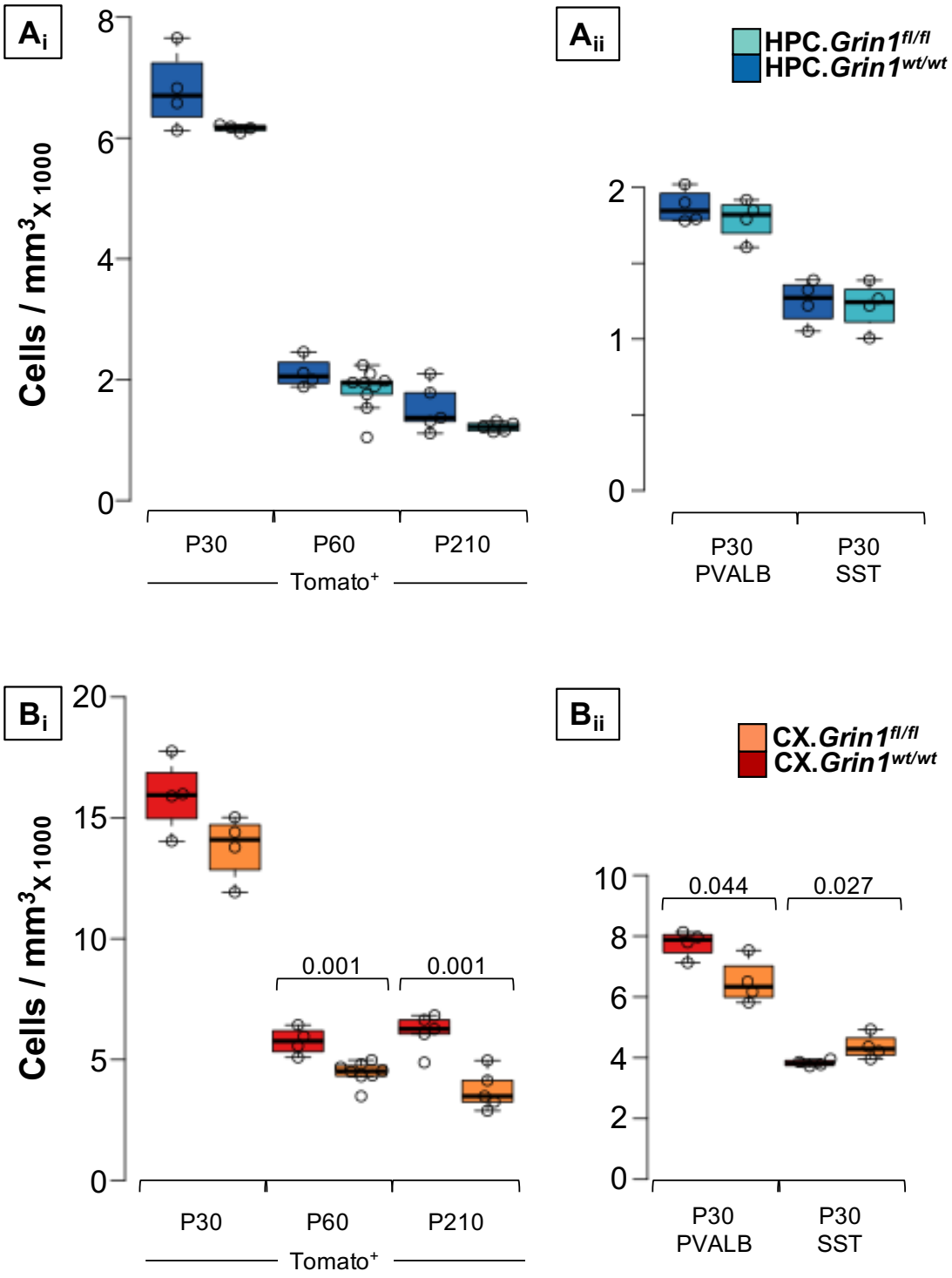

Figure 13: **Figure2, Supp.1 | MGE subtype abundances upon *Grin1*-ablation** **A,** Boxplots indicating the cell counts of hippocampal MGE-derived interneurons expressing $(\mathbf{A}_i)$ Ai14/tdTomato, $(\mathbf{A}_{ii})$ PV, SST immunostaining from $Grin1^{wt/wt}$and $Grin1^{fl/fl}$ **B,** Boxplots indicating the cell counts of cortical MGE-derived interneurons expressing $(\mathbf{B}_i)$ Ai14/tdTomato, and $(\mathbf{B}_{ii})$ PV, SST immunostaining from $Grin1^{wt/wt}$and $Grin1^{fl/fl}$. t-test for statistical analysis.

A_i

	WT.MGE.CX	NULL.MGE.CX	WT.MGE.HPC	NULL.MGE.HPC
	#cells			
SST.all	4024	946	1532	1108
PVALB.all	1265	286	401	340
NGFC.all	287	100	1032	743
All.MGE	5576	1332	2965	2191

A_{ii}

	WT.MGE.CX	NULL.MGE.CX	WT.MGE.HPC	NULL.MGE.HPC
	#cells			
SST.1	310	201	26	25
SST.2	992	186	262	256
SST.3	667	107	399	420
SST.4	764	90	143	149
SST.5	93	39	87	63
SST.6	853	151	505	103
TH.1	345	172	110	92
SST.all	4024	946	1532	1108
	#cells			
PVALB.1	1112	144	294	226
PVALB.2	115	78	106	107
PVALB.3	38	64	1	7
PVALB.all	1265	286	401	340
	#cells			
NGFC.1	187	85	471	606
NGFC.2	100	15	561	137
NGFC.all	287	100	1032	743

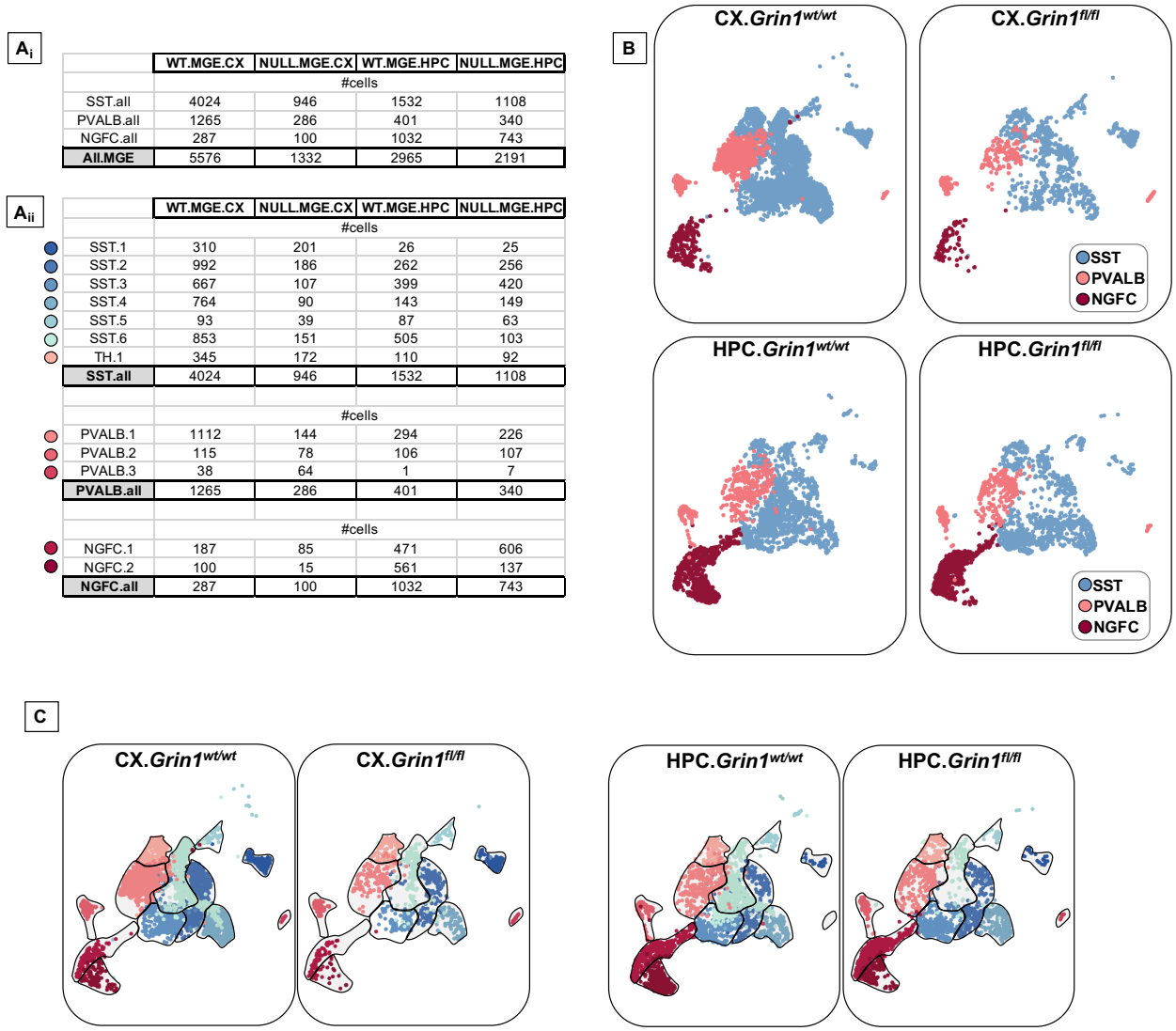

Figure 14: **Figure2, Supp.2 | scRNAseq differential recoveries of MGEsubtypes**
$\mathbf{A}_i$, Number of cells recovered across cardinal subtypes SST, PV and NGFC. $\mathbf{A}_{ii}$, Number of cells recovered within the subtypes of PV / SST/ NGFC. **B,** UMAP representation colored by cardinal MGE-derived interneuron subtypes SST, PVALB and NGFC, highlighting the differential enrichments of cells **C,** Representative UMAP plots indicating the granularity among PV/SST/NGFC subtypes between both brain regions and both genotypes.

of hippocampal neurogliaform cells, Nature Communications 8 (1) (2017) 152–152. doi:10.1038/s41467-017-00218-y.
URL https://dx.doi.org/10.1038/s41467-017-00218-y
[10] J. H. Cornford, M. S. Mercier, M. Leite, V. Magloire, M. Häusser, D. M. Kullmann, Dendritic NMDA receptors in parvalbumin neurons enable strong and stable neuronal assemblies (2019). doi:10.7554/elife.49872.
URL https://dx.doi.org/10.7554/elife.49872
[11] N. V. D. M. García, R. Priya, S. N. Tuncdemir, G. Fishell, T. Karayannis, Sensory inputs control

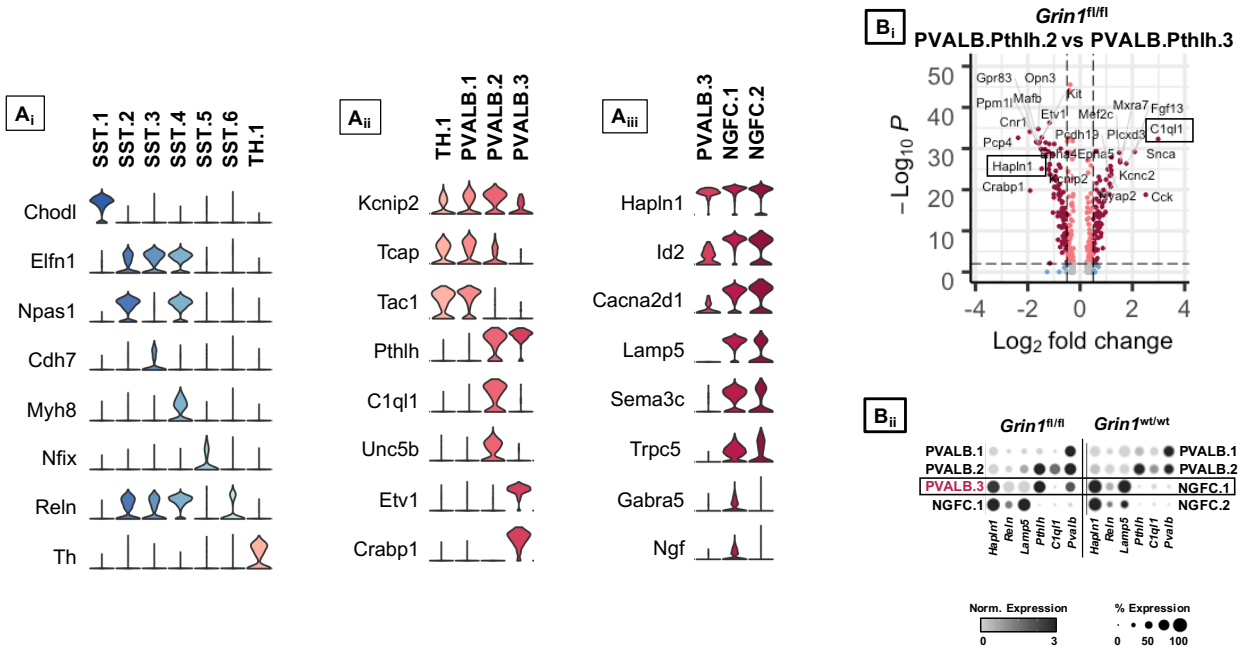

Figure 15: **Figure2, Supp.3 | Select marker gene expression across the subtypes of merged MGE-derived interneurons from *Grin1*$^{wt/wt}$ and *Grin1*$^{fl/fl}$ A,** Violin plot showing the distribution of expression levels of well-known representative cell-type-enriched marker genes across the MGE subtypes. **B**$_i$**,** −log10 False Discovery Rate (FDR) versus log2 fold change (FC) between *Pthlh*-PVALB.2 and *Pthlh*-PVALB.3 at a fold change ≥0.5 and FDR <10e-3. **B**$_{ii}$**,** Dot plots representing the normalized expressions of NGFC marker genes mis expressed in *Pthlh*-PVALB.3 upon *Grin1*-ablation.

the integration of neurogliaform interneurons into cortical circuits, Nature Neuroscience 18 (3) (2015) 393–401. doi:10.1038/nn.3946.
URL https://dx.doi.org/10.1038/nn.3946

[12] J. A. Matta, K. A. Pelkey, M. T. Craig, R. Chittajallu, B. W. Jeffries, C. J. McBain, Developmental origin dictates interneuron AMPA and NMDA receptor subunit composition and plasticity, Nature Neuroscience 16 (8) (2013) 1032–1041. doi:10.1038/nn.3459.
URL https://dx.doi.org/10.1038/nn.3459

[13] R. Luján, R. Shigemoto, G. López-Bendito, Glutamate and GABA receptor signalling in the developing brain, Neuroscience 130 (3) (2005) 567–580. doi:10.1016/j.neuroscience.2004.09.042.
URL https://dx.doi.org/10.1016/j.neuroscience.2004.09.042

[14] J. B. Manent, Glutamate Acting on AMPA But Not NMDA Receptors Modulates the Migration of Hippocampal Interneurons, Journal of Neuroscience 26 (22) (2006) 5901–5909. doi:10.1523/jneurosci.1033-06.2006.
URL https://dx.doi.org/10.1523/jneurosci.1033-06.2006

[15] J. M. Soria, Receptor-activated Calcium Signals in Tangentially Migrating Cortical Cells, Cerebral Cortex 12 (8) (2002) 831–839. doi:10.1093/cercor/12.8.831.
URL https://dx.doi.org/10.1093/cercor/12.8.831

[16] E. Hanson, M. Armbruster, L. A. Lau, M. E. Sommer, Z.-J. Klaft, S. A. Swanger, S. F. Traynelis, S. J. Moss, F. Noubary, J. Chadchankar, C. G. Dulla, Tonic Activation of GluN2C/GluN2D-Containing NMDA Receptors by Ambient Glutamate Facilitates Cortical Interneuron Maturation, The Journal of Neuroscience 39 (19) (2019) 3611–3626. doi:10.1523/jneurosci.1392-18.2019.
URL https://dx.doi.org/10.1523/jneurosci.1392-18.2019

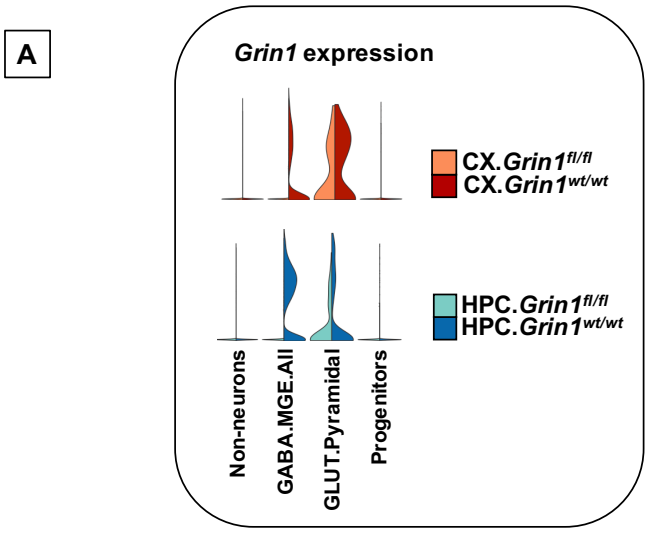

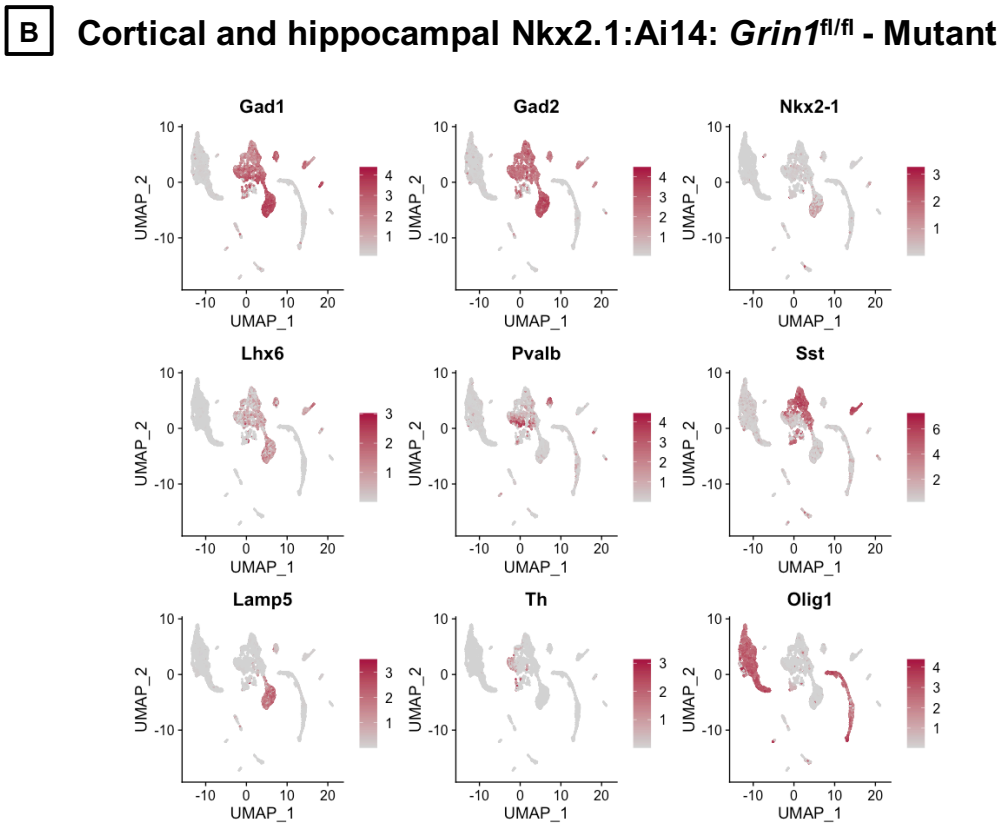

Figure 16: **Figure2, Supp.4 | Expression of control genes in the MGE subtypes subsequent to *Grin1*-ablation**

A$_i$**,** Split-violin plot from both genotypes indicating the expression of *Grin1* in the MGE-derived interneurons, pyramidal neurons and non-neurons. **B,** Representative UMAP plots of cardinal MGE markers genes.

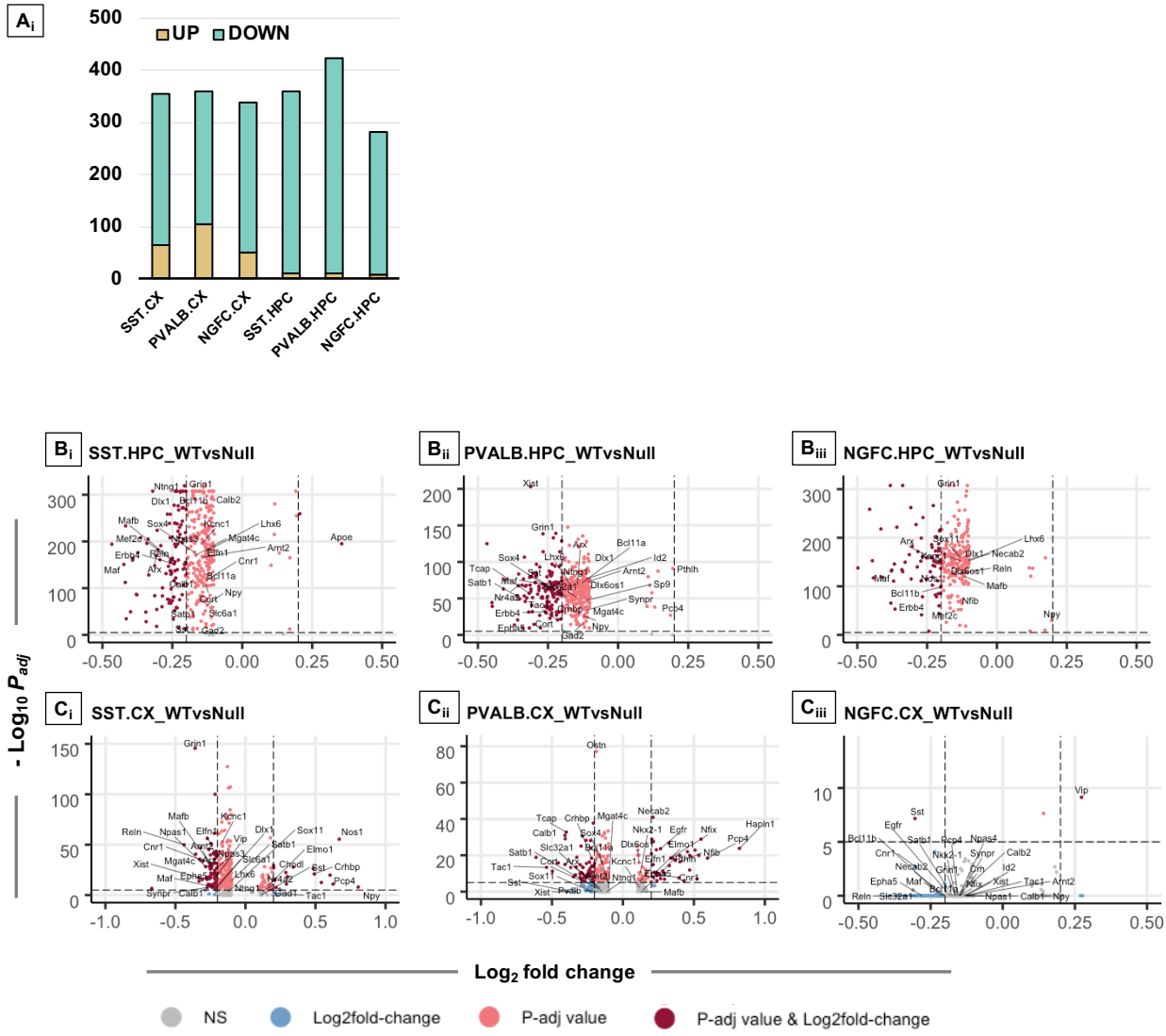

Figure 17: **(Figure3, Supp.1) | Differential gene expression in the MGE subtypes subsequent to *Grin1*-ablation A$_i$,** Split-violin plot from both genotypes indicating the expression of *Grin1* in the MGE-derived interneurons, pyramidal neurons and non-neurons. **A** $_{ii}$ **,** Bar plot denoting the number of genes up/downregulated in the cortical and hippocampal MGE clusters. Volcano plot representing the −log10 False Discovery Rate (FDR) versus log2 fold change (FC) between **B,** hippocampal and **C,**cortical MGE cardinal clusters upon *Grin1*-loss, at a fold change ≥0.2 and FDR <10e-6.

[17] W. Kelsch, Z. Li, S. Wieland, O. Senkov, A. Herb, C. Gongrich, H. Monyer, GluN2B-Containing NMDA Receptors Promote Glutamate Synapse Development in Hippocampal Interneurons, Journal of Neuroscience 34 (48) (2014) 16022–16030. doi:10.1523/jneurosci.1210-14.2014.
URL https://dx.doi.org/10.1523/jneurosci.1210-14.2014

[18] G. Akgül, C. J. McBain, AMPA receptor deletion in developing MGE-derived hippocampal interneurons causes a redistribution of excitatory synapses and attenuates postnatal network oscillatory activity, Scientific Reports 10 (1) (2020) 1333–1333. doi:10.1038/s41598-020-58068-6.
URL https://dx.doi.org/10.1038/s41598-020-58068-6

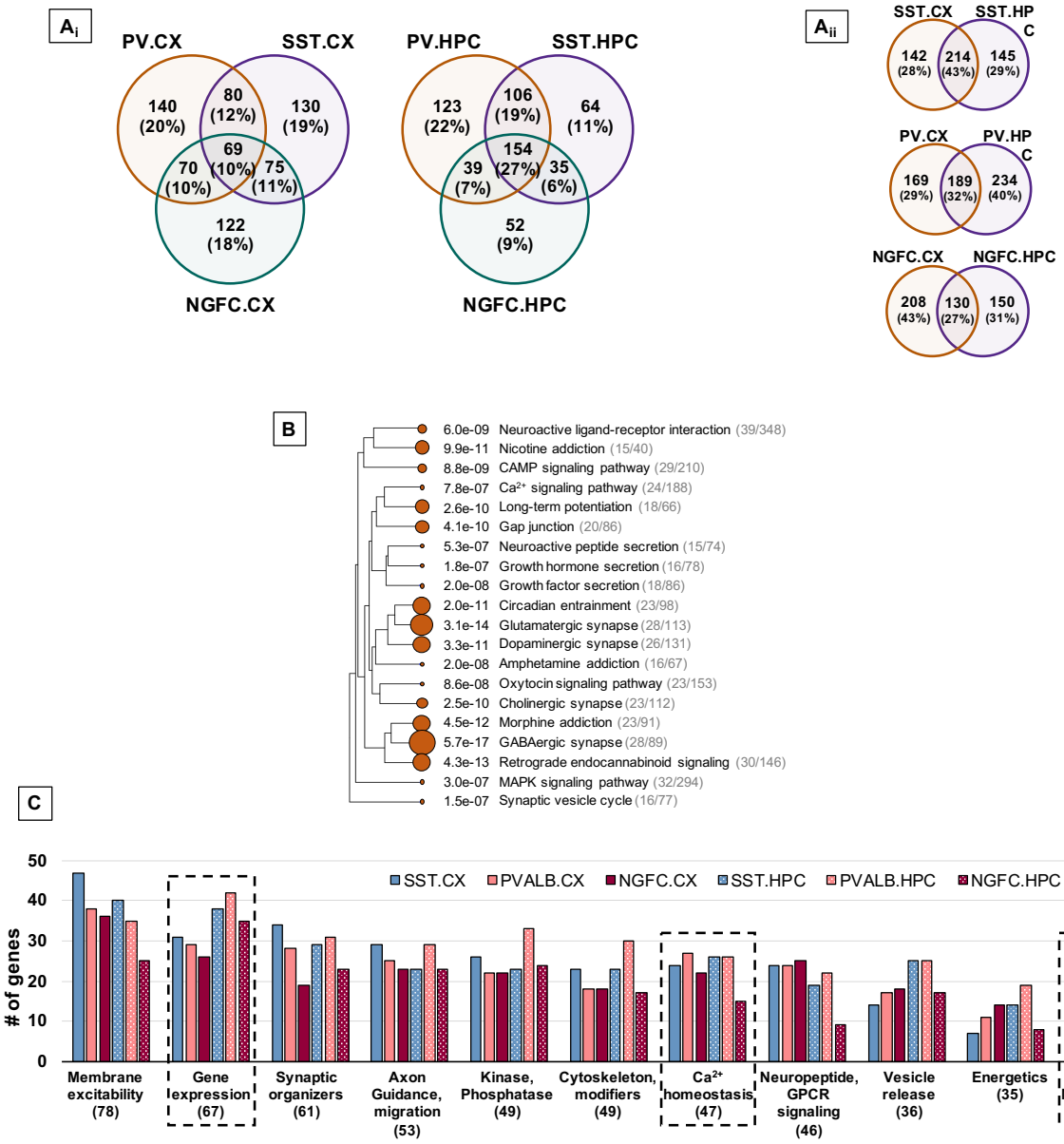

Figure 18: **(Figure3, Supp.2) | Molecular pathways differentially expressed in MGE subtypes** $\mathbf{A_i}$, Venn-diagrams indicating the percentages of DEGs common within MGE subtypes from cortex or hippocampus. $\mathbf{A}_{ii}$, Venn-diagrams indicating the percentages of DEGs common within MGE subtypes from cortex and hippocampus. **B**, Hierarchical clustering tree summarizing the correlation among significant pathways enriched among the DEGs. Pathways with many shared genes are clustered together. Bigger dots indicate more significant P-values. **C**, Bar plot showing the classification of molecular functions of the DEGs, across the MGE subtypes. Total number of DEGs in the particular molecular class indicated in parentheses.

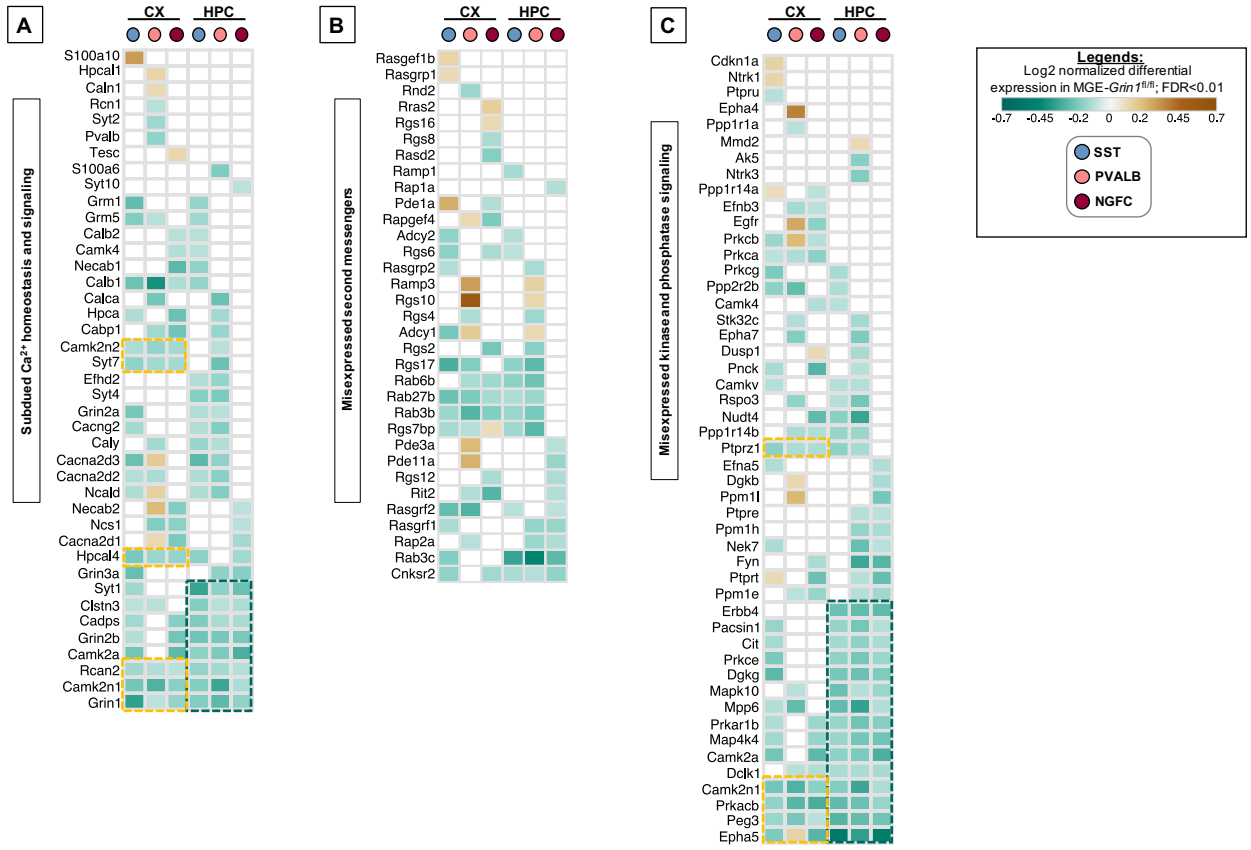

Figure 19: **(Figure4, Supp.1) | Differential expression of intracellular signaling cascades across subtypes upon *Grin1* -ablation** Heatmap of log2 FC of significant DEGs in cortical and hippocampal MGE cardinal subtypes, showing a subset of **A**, genes regulating intracellular Ca^{2+} homeostasis and Ca^{2+} binding proteins; **B**, notable second messengers; and, **C**, Ca^{2+} dependent / activated kinases and phosphatases.

[19] D. Bortone, F. Polleux, KCC2 Expression Promotes the Termination of Cortical Interneuron Migration in a Voltage-Sensitive Calcium-Dependent Manner, Neuron 62 (1) (2009) 53–71. doi:10.1016/j.neuron.2009.01.034.
URL https://dx.doi.org/10.1016/j.neuron.2009.01.034

[20] C. L. Magueresse, H. Monyer, GABAergic Interneurons Shape the Functional Maturation of the Cortex, Neuron 77 (3) (2013) 388–405. doi:10.1016/j.neuron.2013.01.011.
URL https://dx.doi.org/10.1016/j.neuron.2013.01.011

[21] N. V. D. M. García, T. Karayannis, G. Fishell, Neuronal activity is required for the development of specific cortical interneuron subtypes, Nature 472 (7343) (2011) 351–355. doi:10.1038/nature09865.
URL https://dx.doi.org/10.1038/nature09865

[22] M. Yozu, H. Tabata, N. König, K. Nakajima, Migratory Behavior of Presumptive Interneurons Is Affected by AMPA Receptor Activation in Slice Cultures of Embryonic Mouse Neocortex, Developmental Neuroscience 30 (1-3) (2008) 105–116. doi:10.1159/000109856.
URL https://dx.doi.org/10.1159/000109856

[23] O. Marín, Interneuron dysfunction in psychiatric disorders, Nat. Rev. Neurosci 13 (2012) 107–120.

[24] K. Nakazawa, K. Sapkota, The origin of NMDA receptor hypofunction in schizophrenia, Pharmacology & Therapeutics 205 (2020) 107426–107426. doi:10.1016/j.pharmthera.2019.107426.

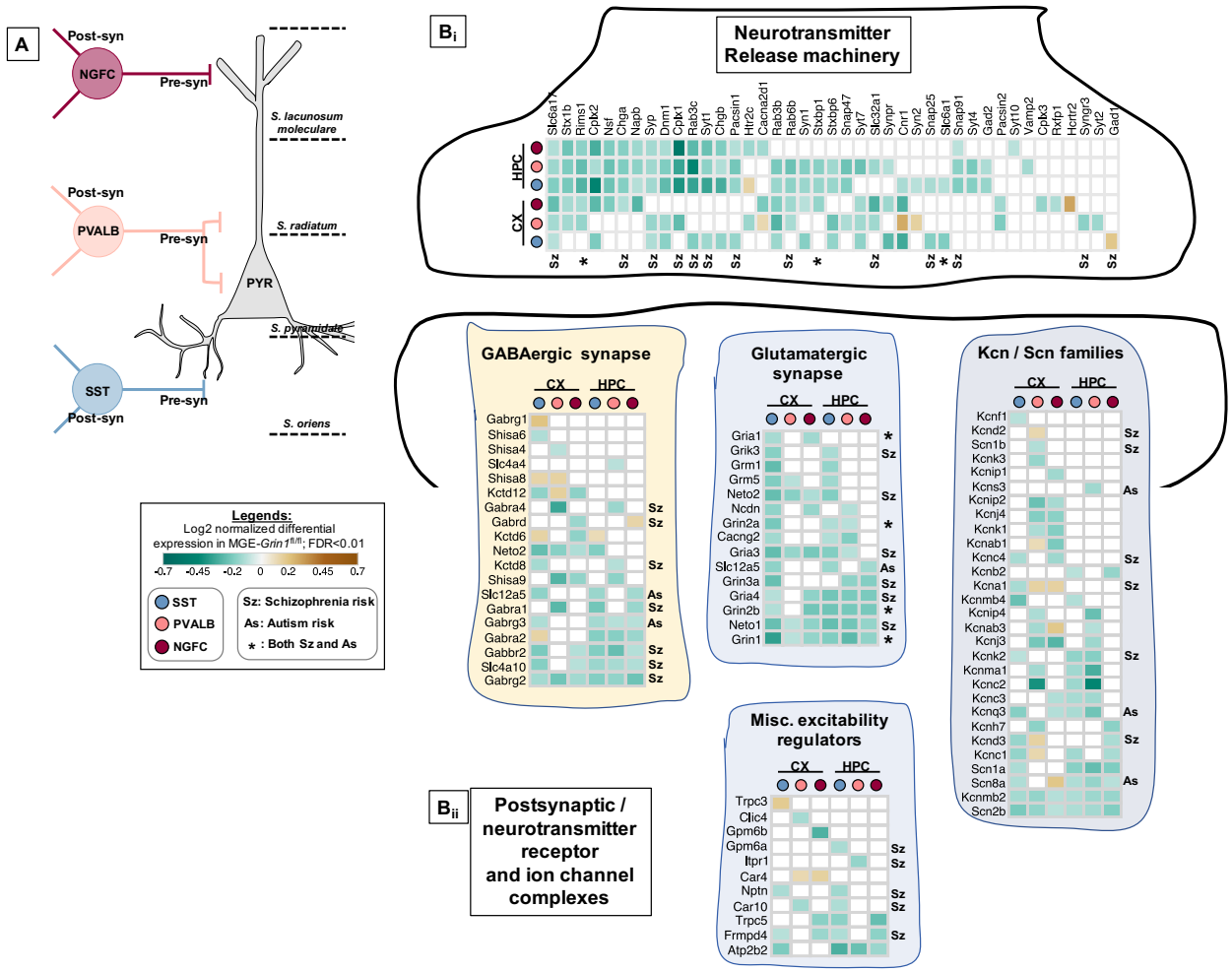

Figure 20: **(Figure6, Supp.1) | Aberrant NMDAR-signaling result in misexpression of regulators of membrane excitability that are high-risk Sz genes** **A**, Schema representing the field of hippocampal pyramidal cell innervated by the interneurons. Heatmap of log2 FC of significant DEGs in cortical and hippocampal MGE cardinal subtypes, showing a subset of $\mathbf{B_i}$, Neurotransmitter release machinery. $\mathbf{B}_{ii}$, Postsynaptic GABA / Glutamate receptor complexes, *Kcn-, Scn-* ion channel complexes and other miscellaneous regulators of excitability.

URL https://dx.doi.org/10.1016/j.pharmthera.2019.107426

[25] B. Rico, O. Marín, Neuregulin signaling, cortical circuitry development and schizophrenia, Current Opinion in Genetics & Development 21 (3) (2011) 262–270. doi:10.1016/j.gde.2010.12.010.
URL https://dx.doi.org/10.1016/j.gde.2010.12.010

[26] A. K. Malhotra, D. A. Pinals, C. M. Adler, I. Elman, A. Clifton, D. Pickar, A. Breier, Ketamine-induced exacerbation of psychotic symptoms and cognitive impairment in neuroleptic-free schizophrenics, Neuropsychopharmacology 17 (1997) 141–150.

[27] H. Homayoun, B. Moghaddam, NMDA Receptor Hypofunction Produces Opposite Effects on Prefrontal Cortex Interneurons and Pyramidal Neurons, Journal of Neuroscience 27 (43) (2007) 11496–11500. doi:10.1523/jneurosci.2213-07.2007.
URL https://dx.doi.org/10.1523/jneurosci.2213-07.2007

[28] R. Nguyen, M. D. Morrissey, V. Mahadevan, J. D. Cajanding, M. A. Woodin, J. S. Yeomans,

K. Takehara-Nishiuchi, J. C. Kim, Parvalbumin and GAD65 Interneuron Inhibition in the Ventral Hippocampus Induces Distinct Behavioral Deficits Relevant to Schizophrenia, Journal of Neuroscience 34 (45) (2014) 14948–14960. doi:10.1523/jneurosci.2204-14.2014.
URL https://dx.doi.org/10.1523/jneurosci.2204-14.2014

[29] J. E. Belforte, V. Zsiros, E. R. Sklar, Z. Jiang, G. Yu, Y. Li, E. M. Quinlan, K. Nakazawa, Postnatal NMDA receptor ablation in corticolimbic interneurons confers schizophrenia-like phenotypes, Nature Neuroscience 13 (1) (2010) 76–83. doi:10.1038/nn.2447.
URL https://dx.doi.org/10.1038/nn.2447

[30] T. Korotkova, E. C. Fuchs, A. Ponomarenko, J. von Engelhardt, H. Monyer, NMDA Receptor Ablation on Parvalbumin-Positive Interneurons Impairs Hippocampal Synchrony, Spatial Representations, and Working Memory, Neuron 68 (3) (2010) 557–569. doi:10.1016/j.neuron.2010.09.017.
URL https://dx.doi.org/10.1016/j.neuron.2010.09.017

[31] V. M. Tatard-Leitman, C. R. Jutzeler, J. Suh, J. A. Saunders, E. N. Billingslea, S. Morita, R. White, R. E. Featherstone, R. Ray, P. I. Ortinski, A. Banerjee, M. J. Gandal, R. Lin, A. Alexandrescu, Y. Liang, R. E. Gur, K. E. Borgmann-Winter, G. C. Carlson, C.-G. Hahn, S. J. Siegel, Pyramidal Cell Selective Ablation of N-Methyl-D-Aspartate Receptor 1 Causes Increase in Cellular and Network Excitability, Biological Psychiatry 77 (6) (2015) 556–568. doi:10.1016/j.biopsych.2014.06.026.
URL https://dx.doi.org/10.1016/j.biopsych.2014.06.026

[32] A. R. Mohn, R. R. Gainetdinov, M. G. Caron, B. H. Koller, Mice with Reduced NMDA Receptor Expression Display Behaviors Related to Schizophrenia, Cell 98 (4) (1999) 427–436. doi:10.1016/s0092-8674(00)81972-8.
URL https://dx.doi.org/10.1016/s0092-8674(00)81972-8

[33] A. M. Bygrave, K. Kilonzo, D. M. Kullmann, D. M. Bannerman, D. Kätzel, Can N-Methyl-D-Aspartate Receptor Hypofunction in Schizophrenia Be Localized to an Individual Cell Type?, Frontiers in Psychiatry 10 (2019) 835–835. doi:10.3389/fpsyt.2019.00835.
URL https://dx.doi.org/10.3389/fpsyt.2019.00835

[34] C. Mayer, C. Hafemeister, R. C. Bandler, R. Machold, R. B. Brito, X. Jaglin, K. Allaway, A. Butler, G. Fishell, R. Satija, Developmental diversification of cortical inhibitory interneurons, Nature 555 (7697) (2018) 457–462. doi:10.1038/nature25999.
URL https://dx.doi.org/10.1038/nature25999

[35] R. Priya, M. F. Paredes, T. Karayannis, N. Yusuf, X. Liu, X. Jaglin, I. Graef, A. Alvarez-Buylla, G. Fishell, Activity Regulates Cell Death within Cortical Interneurons through a Calcineurin-Dependent Mechanism, Cell Reports 22 (7) (2018) 1695–1709. doi:10.1016/j.celrep.2018.01.007.
URL https://dx.doi.org/10.1016/j.celrep.2018.01.007

[36] F. K. Wong, K. Bercsenyi, V. Sreenivasan, A. Portalés, M. Fernández-Otero, O. Marín, Pyramidal cell regulation of interneuron survival sculpts cortical networks, Nature 557 (7707) (2018) 668–673. doi:10.1038/s41586-018-0139-6.

[37] H. Bading, D. Ginty, M. Greenberg, Regulation of gene expression in hippocampal neurons by distinct calcium signaling pathways, Science 260 (5105) (1993) 181–186. doi:10.1126/science.8097060.
URL https://dx.doi.org/10.1126/science.8097060

[38] H. Bading, M. M. Segal, N. J. Sucher, . H. Dudek, ~. Lipton, S. A. Greenberg, M. E (1995).

[39] E. L. Yap, M. E. Greenberg, Activity-Regulated Transcription: Bridging the Gap between Neural Activity and Behavior (2018).
URL https://doi.org/10.1016/j.neuron.2018.10.013

[40] S. Cull-Candy, S. Brickley, M. Farrant, NMDA receptor subunits: diversity, development and disease, Current Opinion in Neurobiology 11 (3) (2001) 327–335. doi:10.1016/s0959-4388(00)00215-4.
URL https://dx.doi.org/10.1016/s0959-4388(00)00215-4

[41] H. Komuro, P. Rakic (1993).

[42] Q. Xu, M. Tam, S. A. Anderson, Fate mapping Nkx2.1-lineage cells in the mouse telencephalon, The Journal of Comparative Neurology 506 (1) (2008) 16–29. doi:10.1002/cne.21529.
URL https://dx.doi.org/10.1002/cne.21529

[43] K. D. Harris, H. Hochgerner, N. G. Skene, L. Magno, L. Katona, C. B. Gonzales, P. Somogyi, N. Kessaris, S. Linnarsson, J. Hjerling-Leffler, Classes and continua of hippocampal CA1 inhibitory neurons revealed by single-cell transcriptomics, PLOS Biology 16 (6) (2018) e2006387–e2006387. doi:10.1371/journal.pbio.2006387.
URL https://dx.doi.org/10.1371/journal.pbio.2006387

[44] A. B. Muñoz-Manchado, C. B. Gonzales, A. Zeisel, H. Munguba, B. Bekkouche, N. G. Skene, P. Lönnerberg, J. Ryge, K. D. Harris, S. Linnarsson, J. Hjerling-Leffler, Diversity of Interneurons in the Dorsal Striatum Revealed by Single-Cell RNA Sequencing and PatchSeq, Cell Reports 24 (8) (2018) 2179–2190.e7. doi:10.1016/j.celrep.2018.07.053.
URL https://dx.doi.org/10.1016/j.celrep.2018.07.053

[45] Y. Tanaka, Y. Tanaka, T. Furuta, Y. Yanagawa, T. Kaneko, The effects of cutting solutions on the viability of GABAergic interneurons in cerebral cortical slices of adult mice, Journal of Neuroscience Methods 171 (1) (2008) 118–125. doi:10.1016/j.jneumeth.2008.02.021.
URL https://dx.doi.org/10.1016/j.jneumeth.2008.02.021

[46] Y. E. Wu, L. Pan, Y. Zuo, X. Li, W. Hong, Detecting Activated Cell Populations Using Single-Cell RNA-Seq, Neuron 96 (2017) 1–27.

[47] A. Butler, P. Hoffman, P. Smibert, E. Papalexi, R. Satija, Integrating single-cell transcriptomic data across different conditions, technologies, and species, Nature Biotechnology 36 (5) (2018) 411–420. doi:10.1038/nbt.4096.
URL https://dx.doi.org/10.1038/nbt.4096

[48] T. Stuart, A. Butler, P. Hoffman, C. Hafemeister, E. Papalexi, W. M. Mauck, Y. Hao, M. Stoeckius, P. Smibert, R. Satija, Comprehensive Integration of Single-Cell Data. Cell (2019).

[49] A. Paul, M. Crow, R. Raudales, M. He, J. Gillis, Z. J. Huang, Transcriptional Architecture of Synaptic Communication Delineates GABAergic Neuron Identity, Cell 171 (3) (2017) 522–539.e20. doi:10.1016/j.cell.2017.08.032.
URL https://dx.doi.org/10.1016/j.cell.2017.08.032

[50] B. Tasic, V. Menon, T. N. T. Nguyen, T. T. K. Kim, T. Jarsky, Z. Yao, B. B. Levi, L. T. Gray, S. A. Sorensen, T. Dolbeare, Adult mouse cortical cell taxonomy revealed by single cell transcriptomics, Nat. Neurosci. advance on (2016) 1–37.

[51] B. Tasic, V. Menon, T. N. T. Nguyen, T. T. K. Kim, T. Jarsky, Z. Yao, B. B. Levi, L. T. Gray, S. A. Sorensen, T. Dolbeare, D. Bertagnolli, J. Goldy, N. Shapovalova, S. Parry, C. C. Lee, K. Smith, A. Bernard, L. Madisen, S. M. Sunkin, M. Hawrylycz, C. Koch, H. Zeng, Z. Yao, C. C. Lee, N. Shapovalova, S. Parry, L. Madisen, S. M. Sunkin, M. Hawrylycz, C. Koch, H. Zeng, Adult mouse cortical cell taxonomy revealed by single cell transcriptomics, Nature Neuroscience advance on (January) (2016) 1–37. doi:10.1038/nn.4216.

[52] J. Winterer, D. Lukacsovich, L. Que, A. M. Sartori, W. Luo, C. Földy, Single-cell RNA-Seq characterization of anatomically identified OLM interneurons in different transgenic mouse lines, European Journal of Neuroscience 50 (11) (2019) 3750–3771. doi:10.1111/ejn.14549.
URL https://dx.doi.org/10.1111/ejn.14549

[53] B. Tasic, Z. Yao, L. T. Graybuck, K. A. Smith, T. N. Nguyen, D. Bertagnolli, J. Goldy, E. Garren, M. N. Economo, S. Viswanathan, Shared and distinct transcriptomic cell types across neocortical areas, Nature 563 (2018) 72–78.

[54] E. Favuzzi, R. Deogracias, A. Marques-Smith, P. Maeso, J. Jezequel, D. Exposito-Alonso, M. Balia, T. Kroon, A. J. Hinojosa, E. F. Maraver, B. Rico, Distinct molecular programs regulate synapse specificity in cortical inhibitory circuits, Science 363 (6425) (2019) 413–417. doi:10.1126/science.aau8977.

[55] R. Priya, M. F. Paredes, T. Karayannis, N. Yusuf, X. Liu, X. Jaglin, I. Graef, A. Alvarez-Buylla, G. Fishell, Activity Regulates Cell Death within Cortical Interneurons through a Calcineurin-Dependent Mechanism., Cell reports 22 (7) (2018) 1695–1709. doi:10.1016/j.celrep.2018.01.007.

[56] S. J. Butt, V. H. Sousa, M. V. Fuccillo, J. Hjerling-Leffler, G. Miyoshi, S. Kimura, G. Fishell, The Requirement of Nkx2-1 in the Temporal Specification of Cortical Interneuron Subtypes, Neuron 59 (5) (2008) 722–732. doi:10.1016/j.neuron.2008.07.031.

URL https://dx.doi.org/10.1016/j.neuron.2008.07.031

[57] D. J. Laurie, P. H. Seeburg, Regional and developmental heterogeneity in splicing of the rat brain NMDAR1 mRNA, The Journal of Neuroscience 14 (5) (1994) 3180–3194. doi:10.1523/jneurosci.14-05-03180.1994.
URL https://dx.doi.org/10.1523/jneurosci.14-05-03180.1994

[58] H. Monyer, N. Burnashev, D. J. Laurie, B. Sakmann, P. H. Seeburg, Developmental and regional expression in the rat brain and functional properties of four NMDA receptors, Neuron 12 (3) (1994) 529–540. doi:10.1016/0896-6273(94)90210-0.
URL https://dx.doi.org/10.1016/0896-6273(94)90210-0

[59] Z. J. Huang, A. Paul, The diversity of GABAergic neurons and neural communication elements, Nature Reviews Neuroscience 20 (9) (2019) 563–572. doi:10.1038/s41583-019-0195-4.
URL https://dx.doi.org/10.1038/s41583-019-0195-4

[60] O. Hobert, I. Carrera, N. Stefanakis, The molecular and gene regulatory signature of a neuron, Trends in Neurosciences 33 (10) (2010) 435–445. doi:10.1016/j.tins.2010.05.006.
URL https://dx.doi.org/10.1016/j.tins.2010.05.006

[61] K. Y. Kwan, N. Sestan, E. S. Anton, Transcriptional co-regulation of neuronal migration and laminar identity in the neocortex, Development 139 (9) (2012) 1535–1546. doi:10.1242/dev.069963.
URL https://dx.doi.org/10.1242/dev.069963

[62] R. Janky, A. Verfaillie, H. Imrichová, B. V. de Sande, L. Standaert, V. Christiaens, G. Hulselmans, K. Herten, M. N. Sanchez, D. Potier, D. Svetlichnyy, Z. K. Atak, M. Fiers, J.-C. Marine, S. Aerts, iRegulon: From a Gene List to a Gene Regulatory Network Using Large Motif and Track Collections, PLoS Computational Biology 10 (7) (2014) e1003731–e1003731. doi:10.1371/journal.pcbi.1003731.
URL https://dx.doi.org/10.1371/journal.pcbi.1003731

[63] S. J. Otto, S. R. McCorkle, J. Hover, C. Conaco, J. J. Han, S. Impey, G. S. Yochum, J. J. Dunn, R. H. Goodman, G. Mandel, A New Binding Motif for the Transcriptional Repressor REST Uncovers Large Gene Networks Devoted to Neuronal Functions, Journal of Neuroscience 27 (25) (2007) 6729–6739. doi:10.1523/jneurosci.0091-07.2007.
URL https://dx.doi.org/10.1523/jneurosci.0091-07.2007

[64] A. Rodenas-Ruano, A. E. Chávez, M. J. Cossio, P. E. Castillo, R. S. Zukin, REST-dependent epigenetic remodeling promotes the developmental switch in synaptic NMDA receptors, Nature Neuroscience 15 (10) (2012) 1382–1390. doi:10.1038/nn.3214.
URL https://dx.doi.org/10.1038/nn.3214

[65] K. Nikouei, A. B. Muñoz-Manchado, J. Hjerling-Leffler, BCL11B/CTIP2 is highly expressed in GABAergic interneurons of the mouse somatosensory cortex, Journal of Chemical Neuroanatomy 71 (2016) 1–5. doi:10.1016/j.jchemneu.2015.12.004.
URL https://dx.doi.org/10.1016/j.jchemneu.2015.12.004

[66] M. Erburu, I. Muñoz-Cobo, T. Diaz-Perdigon, P. Mellini, T. Suzuki, E. Puerta, R. M. Tordera, SIRT2 inhibition modulate glutamate and serotonin systems in the prefrontal cortex and induces antidepressant-like action, Neuropharmacology 117 (2017) 195–208. doi:10.1016/j.neuropharm.2017.01.033.
URL https://dx.doi.org/10.1016/j.neuropharm.2017.01.033

[67] M. Wątroba, D. Szukiewicz, The role of sirtuins in aging and age-related diseases, Advances in Medical Sciences 61 (1) (2016) 52–62. doi:10.1016/j.advms.2015.09.003.
URL https://dx.doi.org/10.1016/j.advms.2015.09.003

[68] N. Sharma, E. A. Pollina, M. A. Nagy, E.-L. Yap, F. A. DiBiase, S. Hrvatin, L. Hu, C. Lin, M. E. Greenberg, ARNT2 Tunes Activity-Dependent Gene Expression through NCoR2-Mediated Repression and NPAS4-Mediated Activation, Neuron 102 (2) (2019) 390–406.e9. doi:10.1016/j.neuron.2019.02.007.
URL https://dx.doi.org/10.1016/j.neuron.2019.02.007

[69] Y. Wu, Y. G. Yao, X. J. Luo, SZDB: A Database for Schizophrenia Genetic Research, Schizophr. Bull 43 (2017) 459–471.

[70] S. Foundation (2018).

[71] A. S. Cristino, S. M. Williams, Z. Hawi, J. Y. An, M. A. Bellgrove, C. E. Schwartz, L. da F Costa, C. Claudianos, Neurodevelopmental and neuropsychiatric disorders represent an interconnected molecular system, Molecular Psychiatry 19 (3) (2014) 294–301. doi:10.1038/mp.2013.16.
URL https://dx.doi.org/10.1038/mp.2013.16

[72] J. Liu, M. Li, X. J. Luo, B. Su, Systems-level analysis of risk genes reveals the modular nature of schizophrenia, Schizophr. Res 201 (2018) 261–269.

[73] K. J. Mitchell, The genetics of neurodevelopmental disease, Curr. Opin. Neurobiol 21 (2011) 197–203.

[74] Y. Sakai, C. A. Shaw, B. C. Dawson, D. V. Dugas, Z. Al-Mohtaseb, D. E. Hill, H. Y. Zoghbi, Protein Interactome Reveals Converging Molecular Pathways Among Autism Disorders, Science Translational Medicine 3 (86) (2011) 86ra49–86ra49. doi:10.1126/scitranslmed.3002166.
URL https://dx.doi.org/10.1126/scitranslmed.3002166

[75] E. Favuzzi, R. Deogracias, A. Marques-Smith, P. Maeso, J. Jezequel, D. Exposito-Alonso, M. Balia, T. Kroon, A. J. Hinojosa, E. F. Maraver, B. Rico, Distinct molecular programs regulate synapse specificity in cortical inhibitory circuits, Science 363 (6425) (2019) 413–417. doi:10.1126/science.aau8977.
URL https://dx.doi.org/10.1126/science.aau8977

[76] R. Dolmetsch, Excitation-Transcription Coupling: Signaling by Ion Channels to the Nucleus, Science Signaling 2003 (166) (2003) pe4–pe4. doi:10.1126/stke.2003.166.pe4.
URL https://dx.doi.org/10.1126/stke.2003.166.pe4

[77] S. M. Cohen, H. Ma, K. V. Kuchibhotla, B. O. Watson, G. Buzsáki, R. C. Froemke, R. W. Tsien, Excitation-Transcription Coupling in Parvalbumin-Positive Interneurons Employs a Novel CaM Kinase-Dependent Pathway Distinct from Excitatory Neurons, Neuron 90 (2) (2016) 292–307. doi:10.1016/j.neuron.2016.03.001.
URL https://dx.doi.org/10.1016/j.neuron.2016.03.001

[78] N. Flames, R. Pla, D. M. Gelman, J. L. R. Rubenstein, L. Puelles, O. Marin, Delineation of Multiple Subpallial Progenitor Domains by the Combinatorial Expression of Transcriptional Codes, Journal of Neuroscience 27 (36) (2007) 9682–9695. doi:10.1523/jneurosci.2750-07.2007.
URL https://dx.doi.org/10.1523/jneurosci.2750-07.2007

[79] L. Lim, D. Mi, A. Llorca, O. Marín, Development and Functional Diversification of Cortical Interneurons, Neuron 100 (2) (2018) 294–313. doi:10.1016/j.neuron.2018.10.009.
URL https://dx.doi.org/10.1016/j.neuron.2018.10.009

[80] N. Dehorter, G. Ciceri, G. Bartolini, L. Lim, I. del Pino, O. Marín, Tuning of fast-spiking interneuron properties by an activity-dependent transcriptional switch, Science 349 (6253) (2015) 1216–1220. doi:10.1126/science.aab3415.
URL https://dx.doi.org/10.1126/science.aab3415

[81] P. Flandin, Y. Zhao, D. Vogt, J. Jeong, J. Long, G. Potter, H. Westphal, J. L. R. Rubenstein, Lhx6 and Lhx8 Coordinately Induce Neuronal Expression of Shh that Controls the Generation of Interneuron Progenitors, Neuron 70 (5) (2011) 939–950. doi:10.1016/j.neuron.2011.04.020.
URL https://dx.doi.org/10.1016/j.neuron.2011.04.020

[82] E. L.-L. Pai, D. Vogt, A. Clemente-Perez, G. L. McKinsey, F. S. Cho, J. S. Hu, M. Wimer, A. Paul, S. F. Darbandi, R. Pla, T. J. Nowakowski, L. V. Goodrich, J. T. Paz, J. L. Rubenstein, Mafb and c-Maf Have Prenatal Compensatory and Postnatal Antagonistic Roles in Cortical Interneuron Fate and Function, Cell Reports 26 (5) (2019) 1157–1173.e5. doi:10.1016/j.celrep.2019.01.031.
URL https://dx.doi.org/10.1016/j.celrep.2019.01.031

[83] A. Stanco, R. Pla, D. Vogt, Y. Chen, S. Mandal, J. Walker, R. F. Hunt, S. Lindtner, C. A. Erdman, A. A. Pieper, S. P. Hamilton, D. Xu, S. C. Baraban, J. L. R. Rubenstein, NPAS1 Represses the Generation of Specific Subtypes of Cortical Interneurons, Neuron 84 (5) (2014) 940–953. doi:10.1016/j.neuron.2014.10.040.
URL https://dx.doi.org/10.1016/j.neuron.2014.10.040

[84] Z. Liu, Z. Zhang, S. Lindtner, Z. Li, Z. Xu, S. Wei, Q. Liang, Y. Wen, G. Tao, Y. You, Sp9 Regulates Medial Ganglionic Eminence-Derived Cortical Interneuron Development, Cereb. Cortex (2018) 1–15.

[85] R. D. Hodge, T. E. Bakken, J. A. Miller, K. A. Smith, E. R. Barkan, L. T. Graybuck, J. L. Close,

B. Long, N. Johansen, O. Penn, Conserved cell types with divergent features in human versus mouse cortex, Nature (2019).

[86] Z. Yao, T. N. Nguyen, C. T. J. Velthoven, Van, J. Goldy, A. E. Sedeno-Cortes, F. Baftizadeh, D. Bertagnolli, T. Casper, K. Crichton, S. L. Ding (2020).

[87] G. Fishell, A. Kepecs, Interneuron Types as Attractors and Controllers (2020). doi:10.1146/annurev-neuro-070918-050421.
URL https://dx.doi.org/10.1146/annurev-neuro-070918-050421

[88] W. Andrews, M. Barber, L. R. Hernadez-Miranda, J. Xian, S. Rakic, V. Sundaresan, T. H. Rabbitts, R. Pannell, P. Rabbitts, H. Thompson, L. Erskine, F. Murakami, J. G. Parnavelas, The role of Slit-Robo signaling in the generation, migration and morphological differentiation of cortical interneurons, Developmental Biology 313 (2) (2008) 648–658. doi:10.1016/j.ydbio.2007.10.052.
URL https://dx.doi.org/10.1016/j.ydbio.2007.10.052

[89] F. Polleux, K. L. Whitford, P. A. Dijkhuizen, T. Vitalis, A. Ghosh, Control of cortical interneuron migration by neurotrophins and PI3-kinase signaling, Development 129 (2002) 3147–3160.

[90] O. Marín, A. Yaron, A. Bagri, M. Tessier-Lavigne, J. L. R. Rubenstein, Sorting of Striatal and Cortical Interneurons Regulated by Semaphorin-Neuropilin Interactions, Science 293 (2001) 872–875.

[91] S. Nobrega-Pereira, O. Marin, Transcriptional Control of Neuronal Migration in the Developing Mouse Brain, Cerebral Cortex 19 (suppl 1) (2009) i107–i113. doi:10.1093/cercor/bhp044.
URL https://dx.doi.org/10.1093/cercor/bhp044

[92] S. Nóbrega-Pereira, N. Kessaris, T. Du, S. Kimura, S. A. Anderson, O. Marín, Postmitotic Nkx2-1 Controls the Migration of Telencephalic Interneurons by Direct Repression of Guidance Receptors, Neuron 59 (5) (2008) 733–745. doi:10.1016/j.neuron.2008.07.024.
URL https://dx.doi.org/10.1016/j.neuron.2008.07.024

[93] A. Stanco, C. Szekeres, N. Patel, S. Rao, K. Campbell, J. A. Kreidberg, F. Polleux, E. S. Anton, Netrin-1- 3 1 integrin interactions regulate the migration of interneurons through the cortical marginal zone, Proceedings of the National Academy of Sciences 106 (18) (2009) 7595–7600. doi:10.1073/pnas.0811343106.
URL https://dx.doi.org/10.1073/pnas.0811343106

[94] A. Steinecke, C. Gampe, G. Zimmer, J. Rudolph, J. Bolz, EphA/ephrin A reverse signaling promotes the migration of cortical interneurons from the medial ganglionic eminence, Development 141 (2) (2014) 460–471. doi:10.1242/dev.101691.
URL https://dx.doi.org/10.1242/dev.101691

[95] G. Zimmer, P. Garcez, J. Rudolph, R. Niehage, F. Weth, R. Lent, J. Bolz, Ephrin-A5 acts as a repulsive cue for migrating cortical interneurons, European Journal of Neuroscience 28 (1) (2008) 62–73. doi:10.1111/j.1460-9568.2008.06320.x.
URL https://dx.doi.org/10.1111/j.1460-9568.2008.06320.x

[96] Z. Shao, H. Noh, W. B. Kim, P. Ni, C. Nguyen, S. E. Cote, E. Noyes, J. Zhao, T. Parsons, J. M. Park, Dysregulated protocadherin-pathway activity as an intrinsic defect in induced pluripotent stem cell-derived cortical interneurons from subjects with schizophrenia, Nat. Neurosci 22 (2019) 229–242.

[97] B. L. Bloodgood, N. Sharma, H. A. Browne, A. Z. Trepman, M. E. Greenberg, The activity-dependent transcription factor NPAS4 regulates domain-specific inhibition, Nature 503 (7474) (2013) 121–125. doi:10.1038/nature12743.
URL https://dx.doi.org/10.1038/nature12743

[98] Y. Lin, B. L. Bloodgood, J. L. Hauser, A. D. Lapan, A. C. Koon, T.-K. Kim, L. S. Hu, A. N. Malik, M. E. Greenberg, Activity-dependent regulation of inhibitory synapse development by Npas4, Nature 455 (7217) (2008) 1198–1204. doi:10.1038/nature07319.
URL https://dx.doi.org/10.1038/nature07319

[99] X. Sun, Lin, Y, Npas4: Linking Neuronal Activity to Memory, Trends Neurosci 39 (2016) 264–275.

[100] I. Spiegel, A. R. Mardinly, H. W. Gabel, J. E. Bazinet, C. H. Couch, C. P. Tzeng, D. A. Harmin, M. E. Greenberg, Npas4 Regulates Excitatory-Inhibitory Balance within Neural Circuits through Cell-Type-Specific Gene Programs, Cell 157 (5) (2014) 1216–1229. doi:10.1016/j.cell.2014.03.058.

URL https://dx.doi.org/10.1016/j.cell.2014.03.058

[101] B. Ataman, G. L. Boulting, D. A. Harmin, M. G. Yang, M. Baker-Salisbury, E.-L. Yap, A. N. Malik, K. Mei, A. A. Rubin, I. Spiegel, E. Durresi, N. Sharma, L. S. Hu, M. Pletikos, E. C. Griffith, J. N. Partlow, C. R. Stevens, M. Adli, M. Chahrour, N. Sestan, C. A. Walsh, V. K. Berezovskii, M. S. Livingstone, M. E. Greenberg, Evolution of Osteocrin as an activity-regulated factor in the primate brain, Nature 539 (7628) (2016) 242–247. doi:10.1038/nature20111.
URL https://dx.doi.org/10.1038/nature20111

[102] B. Lacar, S. B. Linker, B. N. Jaeger, S. R. Krishnaswami, J. J. Barron, M. J. E. Kelder, S. L. Parylak, A. C. M. Paquola, P. Venepally, M. Novotny, Nuclear RNA-seq of single neurons reveals molecular signatures of activation, Nat. Commun 7 (2016) 11022–11022.

[103] C. M. Müller, A. Vlachos, T. Deller, Calcium homeostasis of acutely denervated and lesioned dentate gyrus in organotypic entorhino-hippocampal co-cultures, Cell Calcium 47 (3) (2010) 242–252. doi:10.1016/j.ceca.2009.12.006.
URL https://dx.doi.org/10.1016/j.ceca.2009.12.006

[104] W. XiangWei, Y. Jiang, H. Yuan, De novo mutations and rare variants occurring in NMDA receptors, Current Opinion in Physiology 2 (2018) 27–35. doi:10.1016/j.cophys.2017.12.013.
URL https://dx.doi.org/10.1016/j.cophys.2017.12.013

[105] J. C. Masdeu, J. Dalmau, K. F. Berman, NMDA Receptor Internalization by Autoantibodies: A Reversible Mechanism Underlying Psychosis?, Trends in Neurosciences 39 (5) (2016) 300–310. doi:10.1016/j.tins.2016.02.006.
URL https://dx.doi.org/10.1016/j.tins.2016.02.006

[106] J. Tarabeux, , O. Kebir, J. Gauthier, F. F. Hamdan, L. Xiong, A. Piton, D. Spiegelman, E. Henrion, B. Millet, F. Fathalli, R. Joober, J. L. Rapoport, L. E. DeLisi, E. Fombonne, L. Mottron, N. Forget-Dubois, M. Boivin, J. L. Michaud, P. Drapeau, R. G. Lafrenière, G. A. Rouleau, M. O. Krebs, Rare mutations in N-methyl-D-aspartate glutamate receptors in autism spectrum disorders and schizophrenia, Translational Psychiatry 1 (11) (2011) e55–e55. doi:10.1038/tp.2011.52.
URL https://dx.doi.org/10.1038/tp.2011.52

[107] Y. Yu, Y. Lin, Y. Takasaki, C. Wang, H. Kimura, J. Xing, K. Ishizuka, M. Toyama, I. Kushima, D. Mori, Rare loss of function mutations in N-methyl-d-aspartate glutamate receptors and their contributions to schizophrenia susceptibility, Transl. Psychiatry 8 (2018) 12–12.

[108] W. Chen, C. Shieh, S. A. Swanger, A. Tankovic, M. Au, M. McGuire, M. Tagliati, J. M. Graham, S. Madan-Khetarpal, S. F. Traynelis, H. Yuan, T. M. Pierson, GRIN1 mutation associated with intellectual disability alters NMDA receptor trafficking and function, Journal of Human Genetics 62 (6) (2017) 589–597. doi:10.1038/jhg.2017.19.
URL https://dx.doi.org/10.1038/jhg.2017.19

[109] L. L. Gibson, T. A. Pollak, G. Blackman, M. Thornton, N. Moran, A. S. David, The Psychiatric Phenotype of Anti-NMDA Receptor Encephalitis, The Journal of Neuropsychiatry and Clinical Neurosciences 31 (1) (2019) 70–79. doi:10.1176/appi.neuropsych.17120343.
URL https://dx.doi.org/10.1176/appi.neuropsych.17120343

[110] G. L. Carvill, B. M. Regan, S. C. Yendle, B. J. O'Roak, N. Lozovaya, N. Bruneau, N. Burnashev, A. Khan, J. Cook, E. Geraghty, L. G. Sadleir, S. J. Turner, M.-H. Tsai, R. Webster, R. Ouvrier, J. A. Damiano, S. F. Berkovic, J. Shendure, M. S. Hildebrand, P. Szepetowski, I. E. Scheffer, H. C. Mefford, GRIN2A mutations cause epilepsy-aphasia spectrum disorders, Nature Genetics 45 (9) (2013) 1073–1076. doi:10.1038/ng.2727.
URL https://dx.doi.org/10.1038/ng.2727

[111] J. R. Lemke, D. Lal, E. M. Reinthaler, I. Steiner, M. Nothnagel, M. Alber, K. Geider, B. Laube, M. Schwake, K. Finsterwalder, Mutations in GRIN2A cause idiopathic focal epilepsy with rolandic spikes, Nat. Genet 45 (2013) 1067–1072.

[112] S. J. Dienel, D. A. Lewis, Alterations in cortical interneurons and cognitive function in schizophrenia, Neurobiology of Disease 131 (2019) 104208–104208. doi:10.1016/j.nbd.2018.06.020.
URL https://dx.doi.org/10.1016/j.nbd.2018.06.020

[113] D. A. Lewis, T. Hashimoto, D. W. Volk, Cortical inhibitory neurons and schizophrenia, Nature Reviews Neuroscience 6 (4) (2005) 312–324. doi:10.1038/nrn1648.
URL https://dx.doi.org/10.1038/nrn1648

[114] F. Ali, D. M. Gerhard, K. Sweasy, S. Pothula, C. Pittenger, R. S. Duman, A. C. Kwan, Ketamine disinhibits dendrites and enhances calcium signals in prefrontal dendritic spines, Nature Communications 11 (1) (2020) 72–72. doi:10.1038/s41467-019-13809-8.
URL https://dx.doi.org/10.1038/s41467-019-13809-8

[115] R. Chittajallu, K. Auville, V. Mahadevan, M. Lai, S. Hunt, D. Calvigioni, K. A. Pelkey, K. Zaghloul, C. J. Mcbain (2020).

[116] K. Nakao, V. Jeevakumar, S. Z. Jiang, Y. Fujita, N. B. Diaz, C. A. P. Annan, K. L. E. Jaunarajs, K. Hashimoto, J. E. Belforte, K. Nakazawa (2018).

[117] R. C. Team (2013).

[118] A. Paul, M. Crow, R. Raudales, J. Gillis, Z. J. Huang, Transcriptional Architecture of Synaptic Communication Delineates Cortical GABAergic Neuron Identity, Cell 171 (3) (2017) 522–539. doi:10.1016/j.cell.2017.08.032.

[119] A. Saunders, E. Z. Macosko, A. Wysoker, M. Goldman, F. M. Krienen, H. de Rivera, E. Bien, M. Baum, L. Bortolin, S. Wang, A. Goeva, J. Nemesh, N. Kamitaki, S. Brumbaugh, D. Kulp, S. A. McCarroll, Molecular Diversity and Specializations among the Cells of the Adult Mouse Brain, Cell 174 (4) (2018) 1015–1030.e16. doi:10.1016/j.cell.2018.07.028.
URL https://dx.doi.org/10.1016/j.cell.2018.07.028

[120] Z. Yao, T. N. Nguyen, C. T. J. van Velthoven, J. Goldy, A. E. Sedeno-Cortes, F. Baftizadeh, D. Bertagnolli, T. Casper, K. Crichton, S.-L. Ding, O. Fong, E. Garren, A. Glandon, J. Gray, L. T. Graybuck, D. Hirschstein, M. Kroll, K. Lathia, B. Levi, D. McMillen, S. Mok, T. Pham, Q. Ren, C. Rimorin, N. Shapovalova, J. Sulc, S. M. Sunkin, M. Tieu, A. Torkelson, H. Tung, K. Ward, N. Dee, K. A. Smith, B. Tasic, H. Zeng, A taxonomy of transcriptomic cell types across the isocortex and hippocampal formation, bioRxiv (mar 2020). doi:10.1101/2020.03.30.015214.

[121] G. Finak, A. McDavid, M. Yajima, J. Deng, V. Gersuk, A. K. Shalek, C. K. Slichter, H. W. Miller, M. J. McElrath, M. Prlic, P. S. Linsley, R. Gottardo, MAST: a flexible statistical framework for assessing transcriptional changes and characterizing heterogeneity in single-cell RNA sequencing data, Genome Biology 16 (1) (2015). doi:10.1186/s13059-015-0844-5.
URL https://dx.doi.org/10.1186/s13059-015-0844-5

[122] M. Ximerakis, S. L. Lipnick, B. T. Innes, S. K. Simmons, X. Adiconis, D. Dionne, B. A. Mayweather, L. Nguyen, Z. Niziolek, C. Ozek, V. L. Butty, R. Isserlin, S. M. Buchanan, S. S. Levine, A. Regev, G. D. Bader, J. Z. Levin, L. L. Rubin, Single-cell transcriptomic profiling of the aging mouse brain, Nature Neuroscience 22 (10) (2019) 1696–1708. doi:10.1038/s41593-019-0491-3.
URL https://dx.doi.org/10.1038/s41593-019-0491-3

[123] B. Kevin (2019). [link].
URL Https://Github.Com/Kevinblighe/EnhancedVolcano

[124] S. X. Ge, D. Jung, R. Yao, ShinyGO: a graphical gene-set enrichment tool for animals and plants, Bioinformatics 36 (8) (2020) 2628–2629. doi:10.1093/bioinformatics/btz931.
URL https://dx.doi.org/10.1093/bioinformatics/btz931

[125] K. R. Brown, I. Jurisica, Unequal evolutionary conservation of human protein interactions in interologous networks, Genome Biology 8 (5) (2007) R95–R95. doi:10.1186/gb-2007-8-5-r95.
URL https://dx.doi.org/10.1186/gb-2007-8-5-r95

[126] M. Kotlyar, C. Pastrello, F. Pivetta, A. L. Sardo, C. Cumbaa, H. Li, T. Naranian, Y. Niu, Z. Ding, F. Vafaee, F. Broackes-Carter, J. Petschnigg, G. B. Mills, A. Jurisicova, I. Stagljar, R. Maestro, I. Jurisica, In silico prediction of physical protein interactions and characterization of interactome orphans, Nature Methods 12 (1) (2015) 79–84. doi:10.1038/nmeth.3178.
URL https://dx.doi.org/10.1038/nmeth.3178

[127] C. Stark, BioGRID: a general repository for interaction datasets, Nucleic Acids Research 34 (90001) (2006) D535–D539. doi:10.1093/nar/gkj109.

URL https://dx.doi.org/10.1093/nar/gkj109

[128] V. Mahadevan, C. S. Khademullah, Z. Dargaei, J. Chevrier, P. Uvarov, J. Kwan, R. D. Bagshaw, T. Pawson, A. Emili, Y. D. Koninck (2017).

[129] M. E. Smoot, K. Ono, J. Ruscheinski, P. L. Wang, T. Ideker, Cytoscape 2.8: new features for data integration and network visualization, Bioinformatics 27 (3) (2011) 431–432. doi:10.1093/bioinformatics/btq675.
URL https://dx.doi.org/10.1093/bioinformatics/btq675